Received: 23 December 2022 | Revised: 21 July 2023 | Accepted: 5 August 2023

DOI: 10.1002/hyp.14966

RESEARCH ARTICLE

WILEY

Testing CASE: A new event-based Morgan-Morgan-Finney-type erosion model for different rainfall experimental scenarios

Thomas Brunner[1,2] | Thomas Weninger[1] | Elmar Schmaltz[1] | Josef Krasa[3] | Jakub Stasek[3] | Laura Zavattaro[4] | Istvan Sisak[5] | Tomas Dostal[3] | Andreas Klik[2] | Peter Strauss[1]

[1]Institute for Land and Water Management Research, Federal Agency for Water Management, Petzenkirchen, Austria

[2]Department of Water, Atmosphere and Environment, Institute for Soil Physics and Rural Water Management, University of Natural Resources and Life Sciences, Vienna, Austria

[3]Faculty of Civil Engineering, Czech Technical University in Prague, Prague, Czech Republic

[4]Department of Veterinary Sciences, Università degli Studi di Torino, Torino, Italy

[5]Faculty of Agriculture, University of Szeged, Hódmezővásárhely, Hungary

Correspondence
Thomas Brunner, Institute for Land and Water Management Research, Federal Agency for Water Management, Pollnbergstraße 1, Petzenkirchen 3252, Austria.
Email: thomas.brunner@baw.at

Funding information
Horizon 2020 Framework Programme; EU Financed Projects, Grant/Award Numbers: EVK1-CT-1999-00007, 773903, 101000224

Abstract

Every application of soil erosion models brings the need of proper parameterisation, that is, finding physically or conceptually plausible parameter values that allow a model to reproduce measured values. No universal approach for model parameterisation, calibration and validation exists, as it depends on the model, spatial and temporal resolution and the nature of the datasets used. We explored some existing options for parameterisation, calibration and validation for erosion modelling exemplary with a specific dataset and modelling approach. A new Morgan-Morgan-Finney (MMF)-type model was developed, representing a balanced position between physically-based and empirical modelling approaches. The resulting model termed 'calculator for soil erosion' (CASE), works in a spatially distributed way on the timescale of individual rainfall events. A dataset of 142 high-intensity rainfall experiments in Central Europe (AT, HU, IT, CZ), covering various slopes, soil types and experimental designs was used for calibration and validation with a modified Monte-Carlo approach. Subsequently, model parameter values were compared to parameter values obtained by alternative methods (measurements, pedotransfer functions, literature data). The model reproduced runoff and soil loss of the dataset in the validation setting with R^2_{adj} of 0.89 and 0.76, respectively. Satisfactory agreement for the water phase was found, with calibrated saturated hydraulic conductivity (k_{sat}) values falling within the interquartile range of k_{sat} predicted with 14 different pedotransfer functions, or being within one order of magnitude. The chosen approach also well reflected specific experimental setups contained in the dataset dealing with the effects of consecutive rainfall and different soil water conditions. For the sediment phase of the tested model agreement between calibrated cohesion, literature values and field measurements were only partially in line. The methods we explored may specifically be interesting for use with other MMF-type models, or with similar datasets.

KEYWORDS
CASE, erosion modelling, model calibration, model validation, Morgan-Morgan-Finney model, pedotransfer function, revised Morgan-Morgan-Finney model, surface runoff

1 | INTRODUCTION

Reliably predicting soil erosion rates at the field scale is essential from practical (landowner making field management decisions) and administrative (policy, water resources management, river authorities) considerations. Because of the multiple interactions between the different factors that control the soil erosion process, soil erosion modelling is a common strategy for this purpose. However, application of models in general is not straightforward. It is usually guided by three main questions, (a) which model should be used, (b) which input parameters are available, and (c) how to estimate unknown input parameters for the model?

Established models exist that may estimate long-term soil erosion on plot, hillslope and regional scales, the majority of them based on the modelling concepts of the Universal Soil Loss Equation–(R)USLE or variations of it, as discussed by Bezak et al. (2021) or Kinnell (2010). In fact, although basically developed 50 years ago by Wischmeier and Smith (1978), it certainly remains the most widely used model approach. Soil erosion models are typically categorized using varying denominations like 'empirical', 'semi-empirical', 'process-based', 'process-oriented', 'physically-based', and so forth, which happens according to the view of the respective authors, for example, Bezak et al. (2021), rather than following a definitive system. Classifications based on the temporal and spatial resolutions are more straightforward, usually resulting from the respective resolutions of the model in- or output variables.

Using default (R)USLE technology, it is challenging to explicitly link soil loss and surface runoff following surface flow paths, although some examples of 'hybrid' approaches exist that do so, for example, Alder et al. (2015), Vieira, Dabney, and Yoder (2014), Oost et al. (2000) or Kinnell and Risse (1998). However, these approaches are limited when the influence of upstream management and landscape structure is considered. Kinnell (2010) and Kinnell (2017) examined the ability of (R)USLE models like USLE-M and RUSLE2 to predict individual event soil loss. When surface runoff, sediment and structural connectivities are to be investigated, and event-based soil loss is of interest, models from the (R)USLE family are therefore not the obvious choice among available erosion models. The total sediment yield of a catchment area is frequently dominated by only a few extreme events, as lined out by Edwards and Owens (1991), Boardman (2006), González-Hidalgo et al. (2009), Gonzalez-Hidalgo et al. (2012) or Wang et al. (2022), so we assume that concentrating modelling efforts on these events is a feasible approach. For example, the main cropping regions in Austria, these events mainly occur when the soil is not covered and therefore most prone to soil loss, right after seedbed preparation in spring and early summer (Klik & Eitzinger, 2010; Strauss et al., 1995; Strohmeier et al., 2016). Other annual peaks for soil loss can appear after harvesting summer crops, when uncovered soil meets peak rainfall erosivities (Johannsen et al., 2022; Panagos et al., 2016). Modelling such events necessitates employing a model that works at the timescale of individual rainfall/runoff events, excluding most of the temporally lumped modelling approaches. This also excludes using most of the existing Morgan-Morgan-Finney (MMF; Morgan et al., 1984)-type models, which do not operate event-based either.

Consequently, to simulate single high-intensity rainfall events with spatially explicit surface runoff, we chose to develop a model based on the revised Morgan-Morgan-Finney model (Morgan (2001); RMMF), to which we hereafter refer as the 'CASE' (CAlculator for Soil Erosion) model. RMMF takes an intermediate position within the spectrum of existing soil erosion models, being a process-based model, with moderate demand for input data (Morgan (2001). RMMF is described as 'simple process-based' by Jain and Ramsankaran (2018) as well. Several modifications to the RMMF model have already been implemented:

Choi et al. (2017; DMMF), Eekhout et al. (2018; SPHY-MMF), Peñuela et al. (2018; MMF-TWI), Jain and Ramsankaran (2018) have created spatially distributed (grid-based) model versions, while Morgan and Duzant (2008; MMMF) was designed for slope elements of 10–50 m length.

Morgan and Duzant (2008; MMMF) and Jain and Ramsankaran (2018) operate with annual timesteps. Peñuela et al. (2018; MMF-TWI) use monthly timesteps for runoff and soil loss, but including plant and soil moisture sub-models with daily timesteps. Choi et al. (2017; DMMF) and Eekhout et al. (2018; SPHY-MMF) use daily timesteps.

Apart from these few 'major' RMMF variants, several more exist that contain slight deviations from the original formulation. Each approach has its environmental focus and uses different temporal and spatial resolutions and procedures to collect input parameter values. We know of only one of these variants directly employing an infiltration submodel for runoff calculation, as we do in this study: Eekhout et al. (2018; SPHY-MMF).Others use equations developed for saturation-excess being the dominant mechanism for runoff generation. This is stated by Smith et al. (2018) and Peñuela et al. (2017) in regard to MMF-TWI, and by Choi et al. (2017) for DMMF. Our adapted water-phase is more closely related to those of the KINEROS Woolhiser et al. (1990) and EUROSEM Morgan et al. (1998) models, though simplified.

Whenever applying models, be they spatially lumped or explicit, the estimation of input parameter values becomes an issue. The input data demands rise with model complexity which usually is in contrast to actual (soil) data availability. While some of the soil characteristics needed for erosion modelling may be assumed static for many considerations, others, such as soil water content or saturated hydraulic conductivity (k_{sat}), are highly dynamic locally and temporarily and cannot be estimated by such simple means, though appropriate methods exist, as shown by Hu et al. (2015) or De Lannoy et al. (2006). Because of the limited data availability, selecting parameter values is often done by choosing appropriate pedotransfer functions (PTFs) that allow, for instance, to estimate k_{sat}, from basic soil parameters silt, sand and clay content (Patil and Singh (2016). In the CASE model, k_{sat} is a pivotal parameter controlling runoff generation and consequently affecting soil detachment by runoff and transport capacity of the runoff.

For parameterisation of the models of MMF-type models, different approaches have been followed: Feng et al. (2014), in a Chinese karst environment on a catchment with an area of some 10 km^2, collected undisturbed soil samples and transferred them into model parameters using literature values from Morgan (2005), Morgan and Duzant (2008) and PTFs from Saxton et al. (2006). Vieira, Prats, et al. (2014), on burned forest in Portugal at the plot scale, used rainfall experiments for calibration and validation, and soil water content measured with time-domain reflectometry. López-Vicente et al. (2008) worked on cropland in the Pyrenees at a field scale, using laboratory measurements of k_{sat} and relying on parameters from Morgan (2001). Vigiak et al. (2005), in the East African Highlands in two catchments of few km^2 mainly used field and laboratory measurements. Smith et al. (2018) applied MMF-TWI to four catchments in Scotland up to a an area of 27 km^2 area. On a centennial timescale, they used plant and soil water-related inputs calculated with the SWAT model (Gassman et al., 2007) and PTF's from Hollis et al. (2015). Batista et al. (2019) used plot data within a Generalized Likelihood Uncertainty Estimation (GLUE) framework, as described by Beven and Binley (1992). They mainly focused on the provision of appropriate input parameters. Apart from that, large-scale applications in catchments of size 750–10 000 km^2 by Pandey et al. (2009), Li et al. (2010), Lilhare et al. (2015) and Eekhout et al. (2018) exist. They mainly relied on guide values taken from Morgan et al. (1984), Morgan (2001), Morgan and Duzant (2008), Morgan et al. (1998), but also, for example, applied PTFs from Saxton and Rawls (2006) to the global SoilGrids dataset of Hengl et al. (2017).

Concluding from the studies listed above, most relied at least partly on using PTFs, which seems to be a widespread way of deriving input data. The broad geographic and contextual range of applications also suggests a high flexibility of the RMMF family of models. Looking at the large catchment sizes in some of these studies, one also has to bear in mind that some authors, such as Auerswald et al. (2003); Vente et al. (2013); de Vente and Poesen (2005) or Perrin et al. (2001), claim that model validation of distributed models sensu strictu is not possible except for comparatively small spatial scales. This raises the question of how to go forward about model parameterisation, calibration and validation with inevitably imperfect measurements of input parameters available and bearing in mind that no 'best practice approach' exists. The GLUE framework has been widely used in hydrological studies (Blasone et al., 2008; Mirzaei et al., 2015) as well as with various erosion modelling approaches (Batista et al., 2019; Brazier et al., 2000; Cea et al., 2016; Quinton et al., 2010), and could presumably be applied to the model and data used in this study as well.

Most models with multiple parameters can reproduce any measured values, but the parameter values used for this might not agree with basic soil physical or hydrological understanding, a phenomenon that has been termed 'getting the right answer for the wrong reasons' (Beven, 2012; Govers, 2010; Jetten et al., 2003; Quinton, 1994). Thus, special attention needs to be paid at checking calibrated parameter values for plausibility.

Following these considerations, the research questions we wanted to contribute to were:

1. What options exist to parameterise, calibrate and validate a parsimonious soil erosion model exemplified using the presented model?
2. After calibration and validation, how do the resulting parameter values agree with basic soil physical principles, literature values and other parameter estimation methods?

To this end, a dataset of high-intensity rainfall experiments at the plot scale serves as the basis for this task, a widely-used technique in hydrology and soil erosion research, for example, Morgan (2005) or Fiener, Seibert, and Auerswald (2011). To utilize a high-resolution rainfall data set that is needed for event based model application, we replaced the original runoff calculation of the RMMF model with an infiltration sub-model. To account for spatial heterogeneity in general, we replaced the spatially lumped RMMF approach with a distributed raster grid version.

2 | MATERIALS AND METHODS

Conceptually, we used a model structure based on the revised Morgan-Morgan-Finney model (RMMF), as presented by Morgan (2001). Because of some modifications described subsequently, the model version proposed in this study is termed CASE to distinguish it from the numerous other modifications of the original RMMF model.

2.1 | CASE model structure

Figure 1 provides a schematic overview of the CASE model structure. While the RMMF model was designed for predicting total annual soil loss from field-sized areas on hillslopes, CASE is spatially applied to a raster grid with 1 m cell size and temporarily applied at the scale of individual rainfall events. Thus, CASE may be considered spatially distributed but temporally lumped at the rainfall event scale. The model consists of separate runoff (i.e., calculation of infiltration excess and surface runoff routing) and sediment phases (sediment routing and deposition).

2.2 | CASE water phase

For runoff calculation, the RMMF and MMMF models rely on a calculation of soil water storage capacity with annual timesteps in combination with an empirical parameter of effective hydrological depth of the soil (EHD). We hypothesize that, particularly when focusing on high-intensity rainfall events with a high risk of soil loss, infiltration excess runoff may reasonably be considered as the predominant process in surface runoff generation, where surface depression storage becomes insignificant at high slopes, see Reaney et al. (2014).

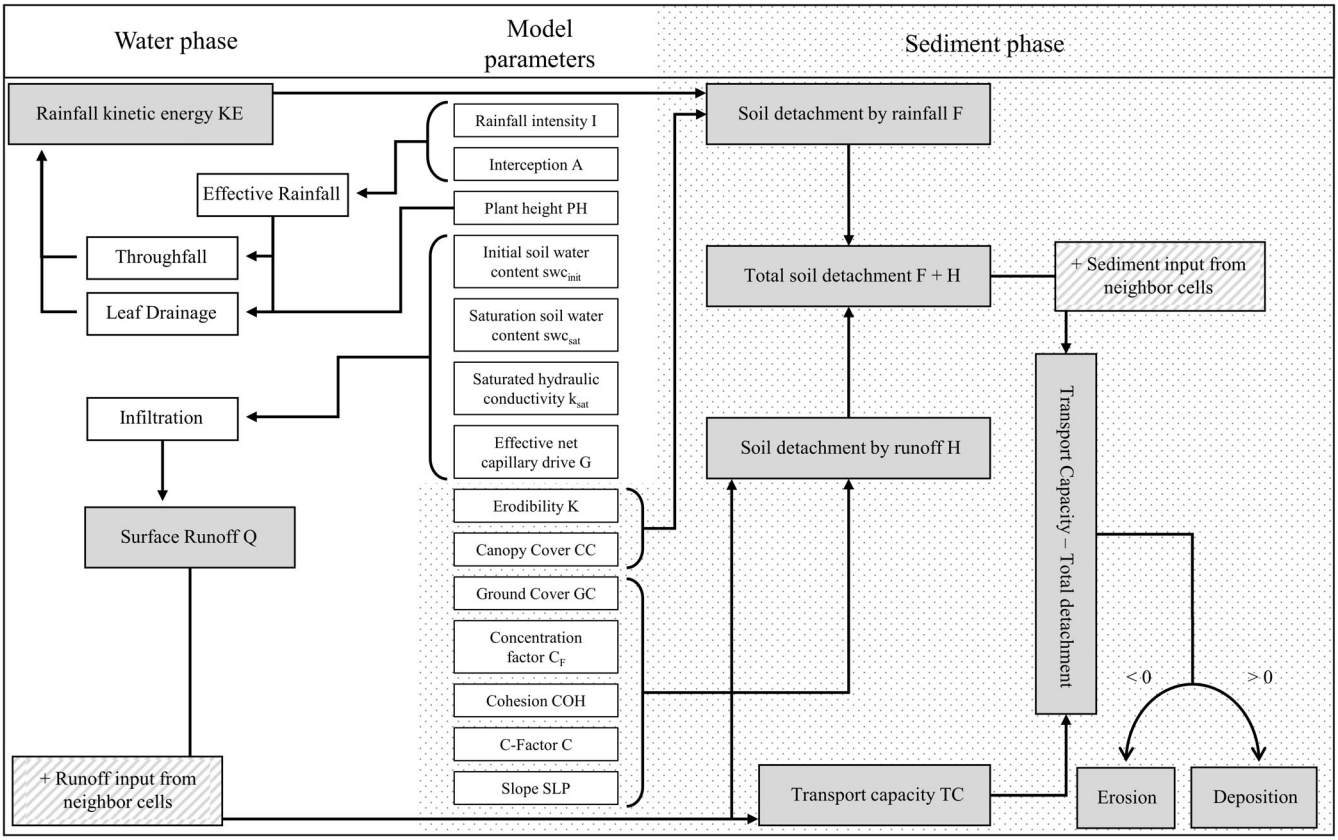

FIGURE 1 Schematic of the CASE model for a single grid cell, separated into water and sediment phase.

To better account for this, the infiltration model of Smith and Parlange (1978), according to Equations (1)–(3) provided by Woolhiser et al. (1990), was implemented. Beven (2021) notes the usefulness of this particular infiltration equation for use with varying rainfall rates, as is the case for part of the dataset used in this study, and even more so for natural rainfall.

$$f_c = k_{sat} \times \frac{\exp(F/B)}{\exp(F/B) - 1} \quad (1)$$

$$B = G\,(\theta_s - \theta_i) \quad (2)$$

$$G = \frac{1}{k_{sat}} \int_{-\infty}^{0} K(\psi)\, d\psi \quad (3)$$

Parameters are infiltration capacity f_c (mm h^{-1}), saturated hydraulic conductivity k_{sat} (mm h^{-1}), effective net capillary drive G (mm), initial soil water content θ_i (%), saturation soil water content θ_s (%), the product of effective net capillary drive and the remaining soil water storage capacity between saturation and current soil water contents B (mm), the amount of rainfall already absorbed in the soil at the current timestep F (mm), the soil matric potential ψ (mm WC) and the hydraulic conductivity function $K(\psi)$ (mm h^{-1}). Rainfall input is required in the form of instantaneous time-intensity pairs, for which we fixed a temporal resolution of 5 min. This was used as a compromise between typically available data and model computational demand.

2.3 | CASE sediment phase

In CASE, the default relationship between the kinetic energy of direct throughfall DT (KE(DT), J m^{-2} mm^{-1}) and rainfall intensity (I, mm h^{-1}) is that of Van Dijk et al. (2002). This relationship is used following Johannsen et al. (2020), who suggested its feasibility for Central European conditions. Other equations may be used if they are considered more feasible for the conditions of other locations.

The model sediment phase is mostly based directly on Morgan (2001) and characterized by a strict separation of rainfall (splash) and runoff (wash) detachment. Effective rainfall is calculated using parameter A as a proportion of total rainfall. Effective rainfall is then split into portions of direct throughfall (DT, mm) and leaf drainage (LD, mm) according to parameter canopy cover (CC, –). Kinetic energies of these rainfall portions are calculated in Equations (4) and (5) and then summed up to give the total detachment by rainfall (F, kg) in Equation (6). KE(DT) is the kinetic energy of direct throughfall (J m^{-2}), DT is the rainfall proportion of direct throughfall (mm), LD is the rainfall proportion of leaf drainage (mm), I is instantaneous rainfall intensity (mm h^{-1}). KE(LD) is the kinetic energy of leaf drainage (J m^{-2}), and PH is plant height (m).

F is the total soil detachment by rainfall (kg), and K is the soil erodibility index (g J^{-1}).

$$KE(DT) = DT \times 28.3I\left(1 - 0.52e^{-0.042I}\right) \quad (4)$$

$$KE(LD) = MAX\left(LD \times \left(\left(15.8 \times PH^{0.5}\right) - 5.87\right), 0\right) \quad (5)$$

$$F = K \times (KE(DT) + KE(LD)) \times 10^{-3} \quad (6)$$

Soil detachment by runoff is calculated separately in Equations (7) and (8). H is the soil detachment by runoff (kg), Z is the soil resistance (kPa), and COH the soil cohesion (kPa), acting only as resistance against runoff detachment in Equation (7), but not against splash detachment. GC is the fraction of ground cover (−), slope is the slope of a particular grid element (°). Similarly, GC affects only runoff detachment, but not rainfall detachment. Z in Equation (8) is proposed by Morgan (2001) based on Rauws and Govers (1988), and COH should be measured at saturated conditions using a torvane.

$$H = Z \times Q^{1.5} \times \mathrm{Sin}\,(\mathrm{slope}) \times (1 - GC) \times 10^{-3} \quad (7)$$

$$Z = \frac{1}{0.5 \times COH} \quad (8)$$

After both rainfall and runoff detachment have been calculated, they are summed up in Equation (9) to give total detachment DET (kg), which represents the sediment available for transport. This available sediment is then compared in Equation (9) with the transport capacity of the runoff (TC, kg). *C* is the USLE management factor C (−), Q is runoff (mm).

$$DET = H + F \quad (9)$$

$$TC = C \times Q^2 \times \mathrm{Sin}\,(\mathrm{slope}) \times 10^{-3} \quad (10)$$

After the calculations of the water phase have been performed (cf. section on spatial discretization), the resulting routed surface runoff Q is used in the remaining equations to calculate detachment by runoff H. H is influenced by slope, GC and Z, and it is summed up with detachment by rainfall into total detachment DET. TC is calculated as well, using the routed surface runoff Q, slope and C. DET and TC are compared in order to ascertain, whether all of the available sediment (=DET) can be transported by the runoff, or not. These assumptions generally follow the assumptions used in RMMF.

The RMMF model does not consider the deposition of eroded soil, in contrast to the more recent MMMF, MMF-TWI and DMMF model versions. In the CASE model, a simplified sediment budget calculation was implemented based on the assumption that deposition (DEP) occurs if the total detachment of a grid element (=sediment available for transport) exceeds its transport capacity (Equation 11), including surface runoff and sediment that the grid element has received from upslope elements.

$$DEP = MIN(DET - TC, 0) \quad (11)$$

2.4 | Spatial representation of the CASE model

The CASE model has been implemented on a grid basis. All calculations are carried out sequentially, starting with the water phase, followed by the downstream accumulation of the runoff and the calculations of the sediment phase. For the sequence of downstream routing, the D8 algorithm by Jenson and Dominque (1988) was implemented, that is, all of the runoff entering a cell is routed to that of the eight neighbouring cells with the highest difference in elevation ('steepest descent'). During runoff routing, no additional infiltration of surface runoff takes place. Therefore, the runoff routing procedure has to be considered as temporally lumped, despite the high temporal resolution of the input rainfall data, and runoff volumes calculated by the model represent the total event runoff volume condensed into a single timestep.

The water phase operates by first applying the infiltration model to each unique combination of rainfall pattern (holding time-intensity pairs, and rainfall parameters calculated from them) and land-use-class (holding all the remaining water and soil phase parameters). The cumulative runoff thus calculated is stored in a lookup dictionary and assigned to each cell according to their rainfall pattern and land use, so that not every cell of the grid has to be calculated individually, which would result in many identical runoff values. After each cell has been assigned a runoff value, a recursive subroutine follows the inverted flow directions upstream, starting at the catchment outlet, to first map out the runoff network, and then follows the flow directions once more in the downstream direction, accumulating the runoff values stored in the individual cells—the result is the 'routed runoff'. Sampling either the routed runoff at the outlet of a catchment, or the maximum value of the resulting grid, gives the total calculated runoff for the catchment, as no second-order infiltration of the routed runoff is calculated.

After routed runoff has been obtained, H and TC are calculated accordingly for each cell. H is summed up with F, and the resulting total DET is compared with TC, to determine whether all the sediment available at a certain cell can be transported, or DEP occurs. Depending on whether net soil loss or sediment yield is the desired output, the resulting erosion values (E) per cell (negative values indicate deposition) can either be summed up or sampled at the catchment outlet.

2.5 | CASE model parameters and where to find them

Model parameters are summarized in Table 1 – parameters not present in the RMMF and MMMF models are indicated. These are

described in more detail in the sections on the water and sediment phases of the model. For the remaining model parameters, guide values and descriptions can be found in Morgan (2001) and Morgan and Duzant (2008). Other suitable sources to derive model parameters may be used, as some are commensurate with parameters used in other erosion models—for instance, Renard et al. (1997), Woolhiser et al. (1990), Beven (2012); Morgan (2005); Seibert and Auerswald (2020).

Before calibration of the water phase, parameter G was linked to k_{sat} based on literature values taken from Woolhiser et al. (1990), using Equation (12) ($R^2 = 0.96$, $n = 11$). When available, G may be derived directly from the soil retention characteristics as Woolhiser et al. (1990) described. However, this information is usually not available, as is the case with the dataset used in this study. Table 2 provides an example of input parameters and their expected ranges taken from different sources.

$$G = 838.53 \times k_{sat}{}^{-0.38} \quad (12)$$

TABLE 1 Model parameter definitions for the CASE model.

Factor	Parameter	Definition
Rainfall	I	Instantaneous rainfall intensity (mm h^{-1})
Soil (top layer)	BD	Bulk density (t m^3)
	swc_{init}	Initial soil water content (% m/m)
	swc_{sat}	Soil water content at saturation (% m/m)
	k_{sat}	Saturated hydraulic conductivity (mm h^{-1})
	G	Effective net capillary drive (mm)
	K	Erodibility (g J^{-1})
	COH	Cohesion (kPa)
Slope	SLP	Slope (°)
Land cover	CC	Canopy cover (–)
	GC	Ground cover (–)
	PH	Plant height (m)
	A	Interception of the rainfall by vegetation cover (–)

Note: Grey shaded rows are parameters that are not present in the original RMMF model.

2.6 | Dataset

The dataset used for this study consists of 142 individual rainfall experiments carried out in CZ, I, AT and HU. All of these experiments were performed shortly after seedbed preparation on bare soil without vegetation. In all experiments, a rainfall simulator described by Strauss et al. (2000) or a similar setup described by Kavka et al. (2015) was used. They represent a range of different rainfall intensities, rainfall durations, slopes, initial soil water contents and soil textures. The general characteristics of the experiments/sites are shown in Table 5. In all experiments, rainfall intensities >50 mm h^{-1} were applied. These intensities represent rainfall events with return intervals >1 year. It seems reasonable for our purpose to concentrate on them to model 'most' of the expected sediment yield.

The experiments can be divided into four different groups A–D, based on the respective experimental design (bottom row in Table 5): Plot dimensions are 5 × 2 m^2 (length × width) for all except group D, where they are 8 × 2 m^2.

A. Experiments at sites SOMO, NAGY, RIVA, TETF, ROTT and RIT ($n = 92$) were performed to evaluate the effect of repeated high-intensity rainfall on runoff and soil loss. Experiments started on initially seedbed-prepared plots and were repeated after 5, 10 and 15 days on the same plot. A constant rainfall intensity of 60 mm h^{-1} was used until steady-state runoff conditions were obtained, which resulted in typical experiment durations of 40–90 min. Presumably due to increasing aggregate dispersion, silting, surface sealing and deteriorating soil resistance, an increased inclination to higher surface runoff and soil loss were experienced with each repeated experiment. Experiments at site SOMO showed

TABLE 2 List of CASE model parameters, likely ranges for Central European conditions, non-exhaustive list of possible sources for parameter values.

Parameter	Label	Typical range	Unit	Source (example)
K	Erodibility	0.05–1.2	g J^{-1}	Morgan (2001)
COH	Cohesion	2–12	kPa	
BD	Bulk density	1.1–15	g cm^{-3}	Morgan and Duzant (2008), PTF from Hollis et al. (2015)
CC	Canopy cover	0–1	(–)	Morgan and Duzant (2008), Renard et al. (1997)
GC	Ground cover	0–1	(–)	
PH	Plant height	0–1	(–)	Morgan (2005), Renard et al. (1997)
C	C-factor	0–1	(–)	
swc_{init}	Initial SWC	0.1–0.6	(–)	–
swc_{sat}	Saturation SWC	0.3–0.6	(–)	PTF from Szabó et al. (2021), Woolhiser et al. (1990)
k_{sat}	Saturated hydraulic conductivity	0.1–500	mm h^{-1}	
g	Effective net capillary drive	0–2000	mm	Woolhiser et al. (1990)

some of the highest totals of soil loss of the whole dataset, having been performed on highly erodible Loess soil, with significant rill erosion visible during the simulation. On the other hand, experiments at site RIT showed the lowest total soil loss.

B. At the STRA site ($n = 6$), experiments were carried out to test the effect of intra-storm varying rainfall intensities on runoff and soil loss. Different rainfall intensity patterns with a peak of 100 mm h^{-1} shifted between the beginning, middle and end of the rainfall experiment were used. The duration of these experiments was kept constant at ca. 70 min. Due to the high peak rainfall intensity applied, STRA experiments are among the highest in total observed soil loss.
C. Experiments at site AN ($n = 6$) are part of a more significant experimental effort with the main focus on the protective effect of cover crops and different tillage/cultivator technologies Hösl and Strauss (2016). From this larger original dataset, only those experiments performed with seedbed conditions for conventional tillage were used. The experiments were carried out until steady state runoff conditions were obtained, with typical durations of 60–90 min and a constant rainfall intensity of 60 mm h^{-1}. Experiments here resulted in comparatively low rates of soil loss, probably due to the soil's high clay content.
D. Experiments at site RI ($n = 38$) are part of a long-term experiment covering a range of crops and crop development stages for calculating the USLE management factors, which is described in detail by Stašek et al. (2023). From this large dataset, only the bare soil reference plots maintained in parallel with the cropped plots were used. These experiments each consisted of a 'dry' and 'wet' run, which were done in sequence on the same day. Typical durations for the experiments were 30–60 min. Rainfall intensity for these experiments was constant at 60 mm h^{-1}.

Apart from the experiments at site RI, all experiments were performed in triplicates. The experiments were grouped at three levels for the model application: Site–Experiment–Replicate. Experiment ID is important where the experiments were performed in sequence.

Instead of using a function to calculate kinetic energy, for the dataset of rainfall experiments used in this work, the equation was substituted with a constant value of 17 J m^{-2} mm^{-1} known for the device used (Strauss et al., 2000).

Concerning the spatial representation of the dataset, all plots were realized as rectangles made of 1 m × 1 m elements, assuming uniform slope, rainfall, and land use conditions.

2.7 | Sensitivity analysis of input parameters

A sensitivity analysis was performed to identify highly sensitive input parameters for model calibration. To assess the parameter sensitivity onto the model outputs (total Q and E), a first estimate of parameter values based on literature for each experiment was varied individually by +/− 20% while the remaining parameters were held constant. The average linear sensitivity (ALS) index was calculated using Equation (13) from Nearing et al. (1990), with I_1 and I_2 being minimum and maximum values of the input, and $\bar{I}$ their average. O_1 and O_2 are the outputs when using these inputs, and $\overline{O}$ their average.

$$\mathrm{ALS} = \frac{\left(\frac{O_2 - O_1}{\overline{O}}\right)}{\left(\frac{I_2 - I_1}{\bar{I}}\right)} \tag{13}$$

2.8 | Calibration and validation methodology

The calibration procedure was done in the form of a 'guided' Monte Carlo simulation and can be considered a simplification of the GLUE method, initially presented by Beven and Binley (1992). A similar procedure is described by Brazier et al. (2001) and Brazier et al. (2000) for the WEPP model. Calibration was performed in sequence, first for the water phase and then using the resulting parameter values in the calibration of the sediment phase—the procedure is shown in Figure 2 and can be described as follows:

1. Decide on the relevant calibration parameters for the soil and water phase based on sensitivity analysis and available measurements – k_{sat}, COH and K.
2. Restrict the parameter space for each calibration parameter to a meaningful range based on model constraints and the location of the experiments.
3. Set up 'expected' parameter values for each experimental site based on expert judgement.
4. Generate a continuous uniform distribution of parameter values within the designated ranges (Table 2), randomly select parameter values out of these distributions and run the model ($n = 5000$–10 000, this was done separately for different ranges of the parameter distributions).
5. Process model outputs and compare modelled with measured Q and E.
6. Choose a parameter combination that gives (a) sufficiently high Nash-Sutcliffe efficiency per site (NSE >0.5), (b) the best fit between modelled and measured total Q and E (+/− 20%), and (c) is closest to the 'expected' parameter value (by sorting and ranking based on mean relative error MRE).

To compare the model outputs to the natural variation within, for example, three experiments performed at the same site, the mean total Q and E per experimental site, consisting of several experiments and replicates, was used as X_{mean} in Equation (14) from Nearing (2000) to calculate NSE. Kinnell (2016) provides valuable insights into plot design in general and the importance of performing replicated experiments due to high variation in measurements on supposedly 'identical' plots.

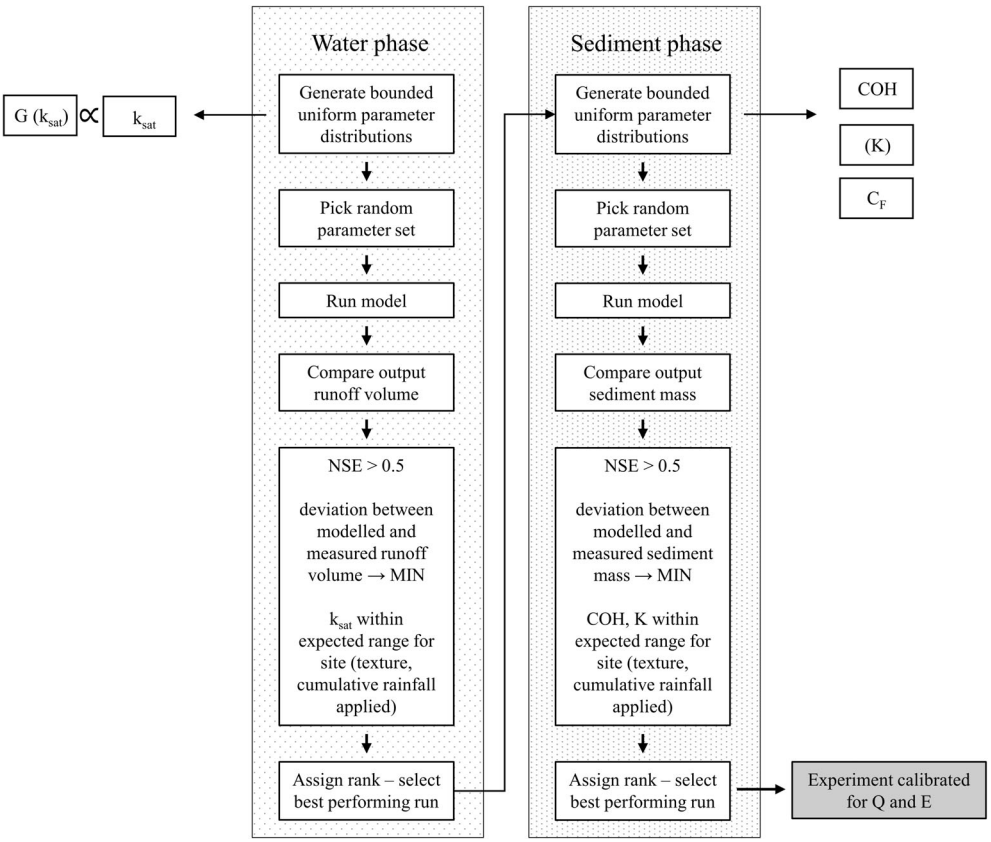

FIGURE 2 Schematic of the CASE calibration procedure for an individual rainfall experiment of the dataset. Parameter abbreviations are given in Table 2, NSE is Nash-Sutcliffe-Efficiency; Q and E are runoff and erosion; parameters on the left and right margins are those chosen for calibration.

$$\mathrm{NSE} = \frac{\sum (X_{\mathrm{obs}} - X_{\mathrm{mean}})^2 - \sum (X_{\mathrm{pred}} - X_{\mathrm{obs}})^2}{\sum (X_{\mathrm{obs}} - X_{\mathrm{mean}})^2} \quad (14)$$

For subsequent model validation, a split-sampling procedure was applied to the dataset. Due to the interrelations between the individual experiments (consecutive rainfall, dry and wet runs – see different experiment groups), it was considered unfeasible to perform a random splitting of the sample, so they were split manually, as considered reasonable for the respective experiment group. The dataset was split per experiment site into 50% of the experiments being used for calibration, and the remaining 50% for validation.

2.8.1 | Introduction of parameter concentration factor C_F

After the first tests on model calibration, it became clear that some of the highest measured sediment losses could not be reached with the default parameters staying within their suggested ranges, as stated in Table 2. This mainly concerned two sites with high susceptibility to rill formation.

At scales such as unit widths of 1 m, the assumption of a homogeneous, uniform sheet of runoff cannot be expected, but full coverage of the cross-section only takes place after a sufficiently large amount of runoff has been generated, as demonstrated, for example, by Peñuela et al. (2013), Appels et al. (2011) or Wang et al. (2018).

A conceptually similar problem was treated by Choi et al. (2017) for the DMMF model, using the relation of the actual runoff velocity to that of an element with standard surface conditions to scale transport capacity accordingly.

To solve this issue, we propose a conceptional 'concentration factor' (C_F) that represents the geometrical relation of the used grid size (typically 1 m) to the total width of a concentrated surface flow path or rills that form during a runoff event. For a cross-section perpendicular to the flow direction, parameter values translate to a runoff volume either extending uniformly across the width of a cell ($C_F = 1$) or concentrating within micro-topographic features, with the surface being only partly inundated ($C_F > 1$)—see Lawrence (1997) for hydraulic considerations. A close relation to various measures of surface roughness can be assumed (Govers et al., 2000; Luo et al., 2020).

Conceptually, C_F is also similar to the reciprocal value of a simplification of the relative surface connection (RSC) function proposed by Antoine et al. (2009) and the subsequent work on it by Peñuela et al. (2013), the latter describing it as an aspect of 'functional connectivity'.

Introduction of the concentration factor C_F changes Equations (7) and (10) for runoff detachment and transport capacity into Equations (15) and (16).

$$H = Z \times (C_F \times Q)^{1.5} \times \mathrm{Sin}\,(\mathrm{slope}) \times (1 - \mathrm{GC}) \times 10^{-3} \quad (15)$$

$$\mathrm{TC} = C \times (C_F \times Q)^2 \times \mathrm{Sin}\,(\mathrm{slope}) \times 10^{-3} \quad (16)$$

3 | RESULTS

3.1 | Sensitivity analysis of input parameters

A sensitivity analysis was performed for all 142 experiments of the calibration dataset (Figure 3). Sensitivities of runoff (Q) and soil loss (E) were calculated separately for each parameter. Since the calibration dataset consists only of bare soil plots without vegetation, some of the model parameters are not relevant for the calibration. Still, they are investigated in the sensitivity analysis. This means that CC, A GC and PH were set to their minimum value of 0, while C was set to its maximum value of 1. For the sensitivity analysis, these were all set to intermediate values of 0.5 instead. Others are highly sensitive but were measured or estimated in each of the calibration experiments (swc_{init}, swc_{sat}).

Nearing (2000) suggested high parameter sensitivity for ALS values ≥1, moderate sensitivity between 0.5 and 1, and low sensitivity for ALS values ≤0.5. These thresholds would translate into high sensitivity concerning Q for parameters swc_{sat}, swc_{init}, k_{sat}, and G, and zero sensitivity for the remaining parameters of the sediment phase. Concerning E, parameters swc_{sat}, swc_{init}, k_{sat} and G show high sensitivity by increasing runoff and therefore increasing runoff detachment and transport capacity. Parameter C_F is highly sensitive as well. Parameters C, K and A show moderate sensitivity, and the remaining parameters COH, GC, CC and PH show low sensitivity. This supports our preliminary assumption of choosing parameter k_{sat} for further calibration of the water phase and COH and C_F for calibrating the sediment phase. The individual results for Q and E show which parameters affect both outputs or only one. Very low sensitivity of plant height (PH) was observed, which casts doubt on the value added by this parameter, at least with low to moderate plant heights <0.70 m.

Overall, the attained positive/negative values of ALS for the different parameters shown in Figure 3 seem sensible from a process point of view. Positive ALS values for swc_{init}, C_F, C, K and PH indicate an increase for Q or E with increasing parameter values. Negative ALS values result for A, GC, COH, CC, G, k_{sat} and swc_{sat}. They indicate a decrease of Q and E with increasing parameter values.

3.2 | Model calibration and validation

The main output of the calibration procedure is shown in Figure 4. The split-off sub-setting of the data set was not done randomly but manually because the individual experiments are not independent, as described in the calibration and validation methodology. For validation, R^2_{adj} of 0.89 (for Q) and 0.76 (for E) could be reached (Figure 4b). Morgan (2005), based on Zhang et al. (1996) and Nearing (1998), notes that R^2 over 0.76 can generally only be reached with highly sophisticated models, and thus, models that yield $R^2 > 0.5$ are deemed acceptable. The results of the calibration that form the basis of Figure 4 and the subsequent figures on individual parameter values are summarized in Supplementary Tables 1 and 2. To elucidate more individual aspects of the calibration/validation procedure, we concentrate on individual model parameters calibrated in the following sections. This is done with the idea that physically implausible parameter values or combinations can still lead to satisfying model outputs. This phenomenon is frequently termed the 'equifinality thesis', for example, in Beven (2006).

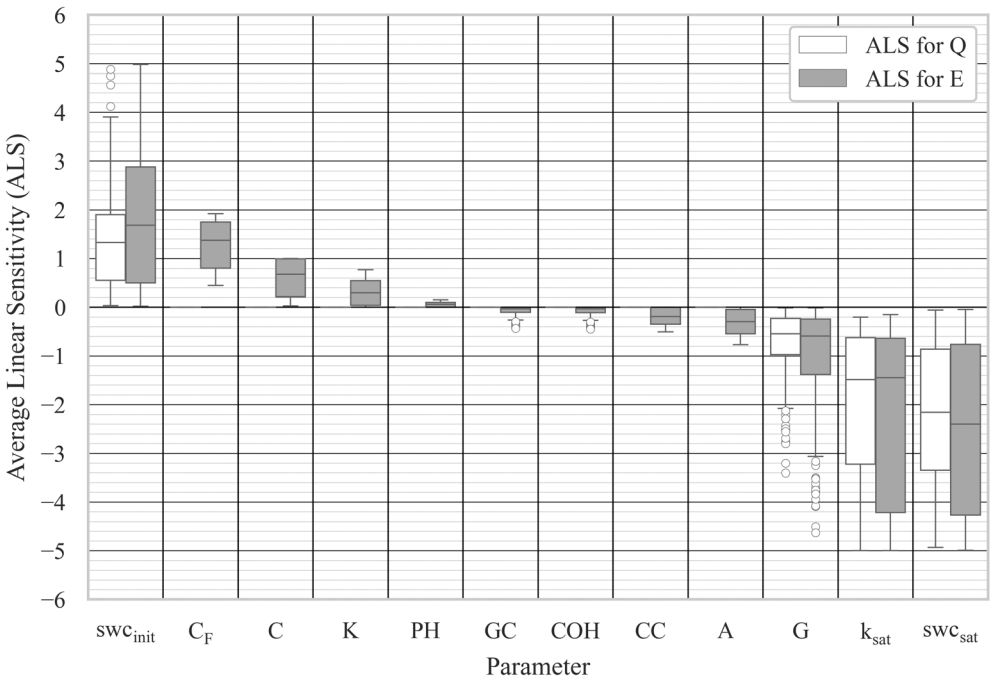

FIGURE 3 Calculation of sensitivity indicator average linear sensitivity (ALS) for the CASE model parameters concerning resulting total runoff (Q) and erosion (E) separately. Each data point is the resulting ALS value for one rainfall experiment; Parameter abbreviations are given in Table 2.

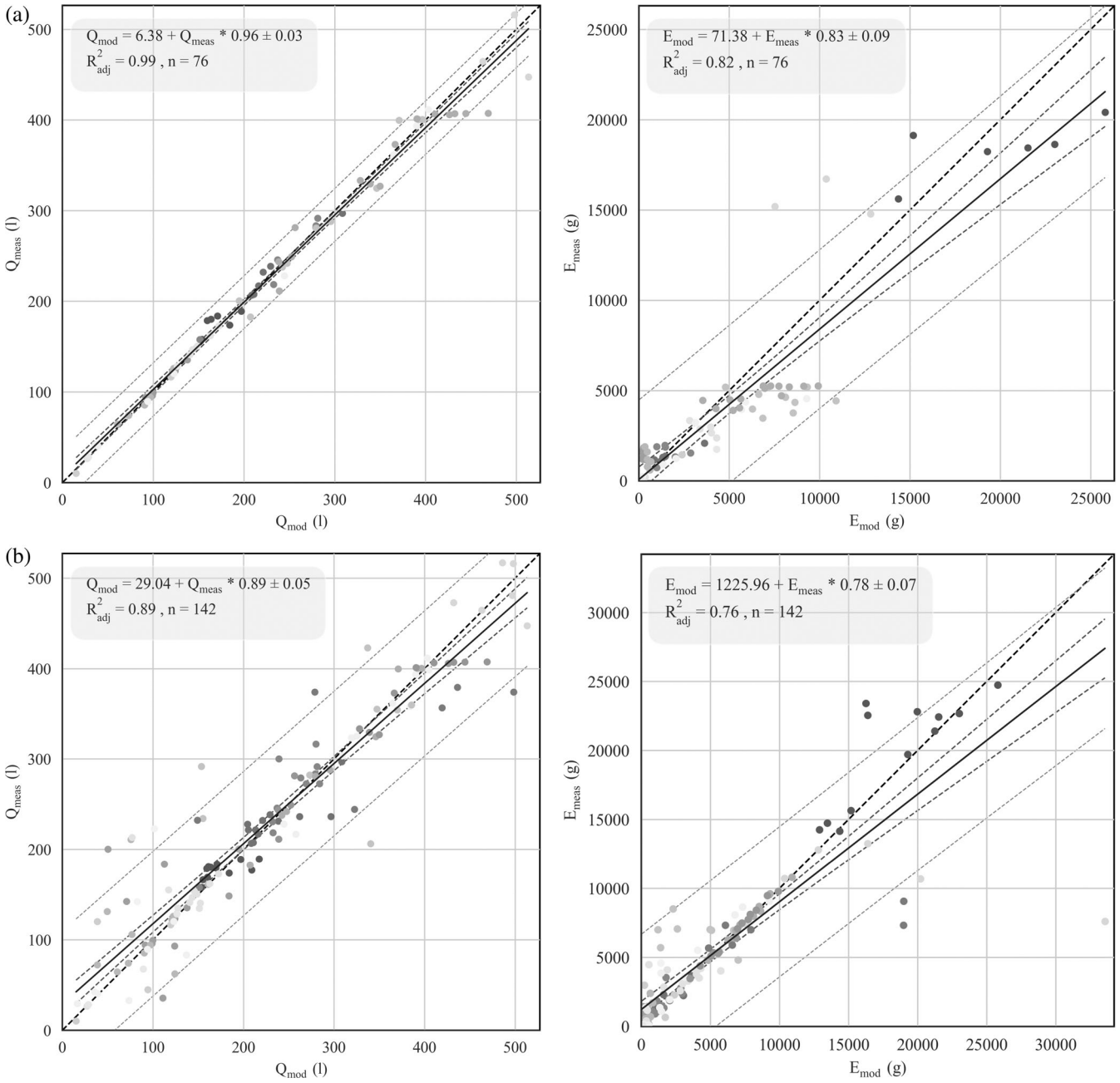

FIGURE 4 Calibration/validation results of the CASE model used on the dataset of 142 rainfall experiments. Top row (a) shows the results of pure calibration for 53% of the dataset; row (b) shows validation for the whole dataset; in both rows, the left figure shows modelled (Q_{mod}) versus measured runoff (Q_{meas}), the right figure shows modelled (E_{mod}) versus measured erosion (E_{meas}), both Q and E are total sums; thick dashed black line is the 1:1 line; solid black line is the resulting linear regression with the stated equation; thick dashed grey lines are the 95% confidence interval of the mean; thin dashed grey lines are the 95% prediction interval.

3.2.1 | Saturated hydraulic conductivity k_{sat} – Agreement with PTFs

Representative values for saturated hydraulic conductivity are notoriously difficult to obtain—measurements are time-consuming, the parameter can be spatially highly variable, and therefore difficult to scale up, as described, for example, by Picciafuoco et al. (2019b). Since a significant change of CASE compared to the original RMMF model consists of the changes in the water phase, it seems appropriate to test the calibrated k_{sat} values for plausibility. In a first attempt, we compared the calibrated k_{sat} values with information suggested by a set of selected PTFs.

Figure 5 shows the calibrated k_{sat} values grouped per experimental site (grey boxplots) and compared to values calculated with 14 different PTFs by Puckett et al. (1985), Dane and Puckett (1994), Ferrer Julià et al. (2004), Cosby et al. (1984), Saxton et al. (1986) Brakensiek

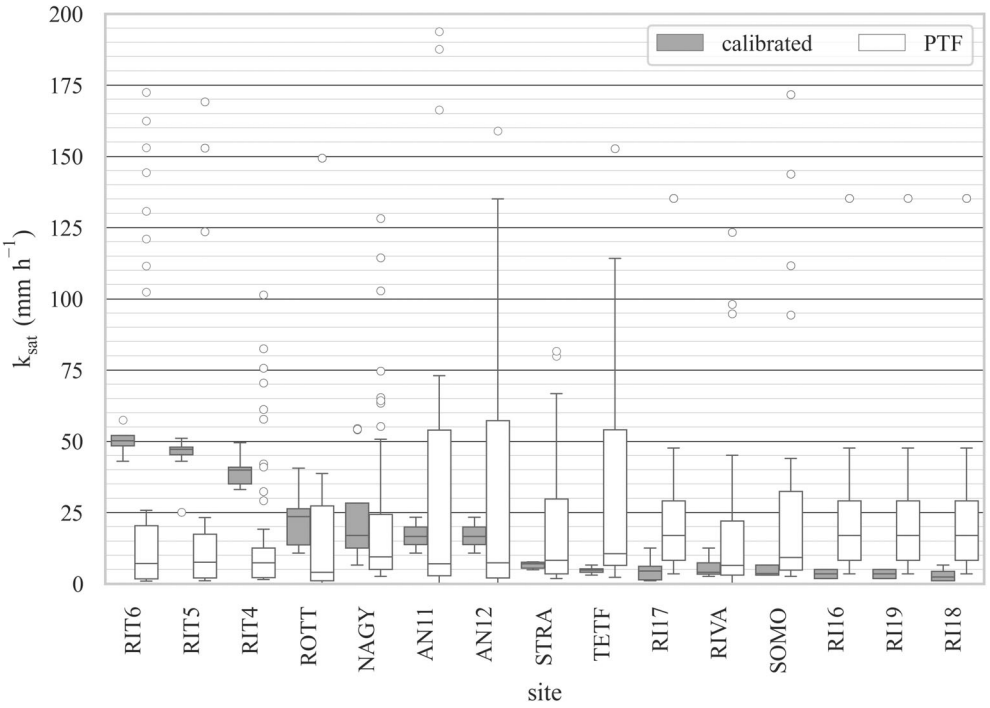

FIGURE 5 k_{sat} values calibrated with the CASE model ('calibrated', grey boxplots) versus k_{sat} values derived from 14 different pedotransfer functions (PTFs) ('PTF', white boxplots) for the experimental sites of the rainfall experiment dataset. Each boxplot represents one experimental site, each data point represents one experiment. The outliers visible are almost exclusively among the PTF values. The y-axis is cut off at 200 mm h^{-1}, there are some outliers from the PTFs above this value.

TABLE 3 Error measures root mean square error (RMSE) and mean relative error (MRE) for the selected pedotransfer functions when predicting the k_{sat} values calibrated with the CASE model for the dataset of rainfall experiments;

Label	References	RMSE (log10 ksat in mm h−1)	MRE (%)	Observations	Parameters
F7	Puckett et al. (1985)	0.95	−6.6	142	C
F8	Dane and Puckett (1994)	0.73	−151.0		C
F9	Ferrer Julià et al. (2004)	0.83	−40.0		SA
F10	Cosby et al. (1984)	0.60	−116.7		C, SA
F12	Brakensiek et al. (1984)	0.81	−131.0		C, SA, SWC_{sat}
F13	Jabro (1992)	1.16	−292.1		C, SI, BD
F16	Ferrer Julià et al. (2004)	0.97	−129.9	115	C, SA, OM
F19	Wösten et al. (2001)	0.94	−241.9	142	C, OM, BD
F20	Vereecken et al. (1990)	0.93	−225.5		C, SA, OM, BD
F21	Weynants et al. (2009)	0.90	3.4		SA, OM, BD
F24	Li et al. (2007)	0.88	−164.8		C, SA, SI, OM, BD
KS01	Szabó et al. (2021)	0.48	−80.3		C, SA, SI, D
KS02	Szabó et al. (2021)	0.54	−56.1		C, SA, SI, D, OM
KS05	Szabó et al. (2021)	0.67	31.3	88	C, SA, SI, D, pH H_2O

Note: Error measures were calculated using $\log_{10}$ of k_{sat} (mm h^{-1}); different numbers of observations are partly due to data availability, partly due to resulting negative k_{sat} predictions.
Abbreviations: BD, bulk density; C, clay; D, sampling depth; OM, organic matter; SA, sand; SI, silt; SWC_{sat}, saturation soil water content.

et al. (1984), Jabro (1992), Wösten et al. (2001), Vereecken et al. (1990), Weynants et al. (2009), Wösten et al. (1999), Li et al. (2007) and Szabó et al. (2021). The results of these individual PTF calculations were lumped together to achieve a range of possible k_{sat} values per experimental site, as typically, only one set of input parameters per site is available. Figure 5 shows that the k_{sat} values obtained with the PTFs exhibit more than 2 orders of magnitude variation. The k_{sat} values obtained with calibration either fall directly within the interquartile range of the PTF calculations (sites ROTT, NAGY, AN11, AN12, STRA, RIVA, SOMO) or are within one order of magnitude of the median predicted by the PTFs (all remaining sites).

To evaluate which of the PTFs performs best at predicting the calibrated values, we compared root mean square error (RMSE) and mean relative error (MRE) for each of the PTFs as discussed by Nasta et al. (2021), which are shown in Table 3. The numbers of observations differ for several reasons (data availability, negative predicted k_{sat} values). These are shown as well as the parameters used in the prediction.

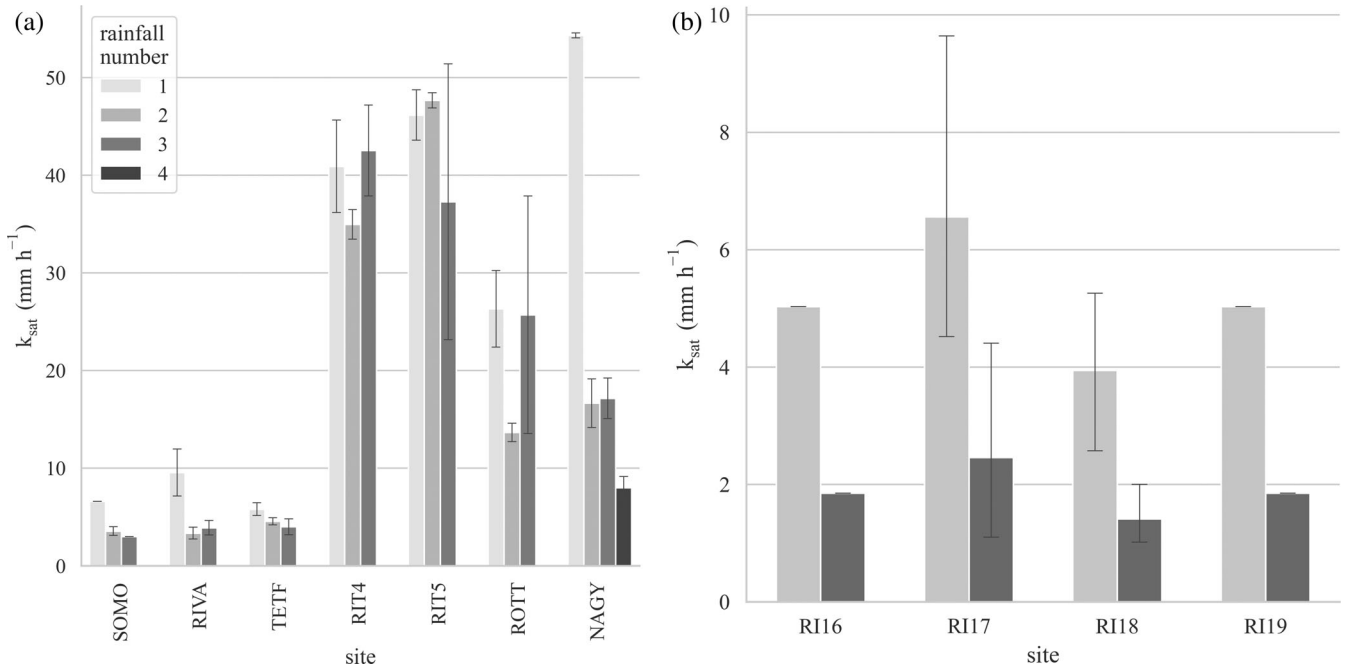

FIGURE 6 k_{sat} values calibrated with the CASE model for specific groups of the rainfall experiments; (a) experiments from group A, with repeated rainfall experiments (b) experiments from group D, with dry (light grey) and wet (dark grey) initial soil water status, aggregated per year for the period 2016–2019; NAGY is the only site where four consecutive experiments were performed; experiments from groups B and C are not included.

3.2.2 | Saturated hydraulic conductivity k_{sat} – Repeated rainfall experiments group A

In the next step, we were interested in the effect of the different groups of experiments on k_{sat} values (bottom row in Table 5). Panel (a) of Figure 6 provides calibrated k_{sat} values for experiments of group A in the sequence of the repeated rainfall applied. Results for sites SOMO, RIVA, TETF, RIT5, and NAGY show lower k_{sat} values for each last experiment (sequential number 3 or 4). The remaining sites RIT4 and ROTT show similar k_{sat} values for the first and last experiments, albeit with high variations. As there are only 12 experiments in group B and C, and there is no reason to expect systematic intra-group variations of k_{sat} values, these are not investigated here.

3.2.3 | Saturated hydraulic conductivity k_{sat} – Dry and wet rainfall experiments group D

Experiments from group D (site RI16-19) each consisted of a dry and corresponding wet experiment. The different swc_{init} and the calibrated k_{sat} values are shown in Supplementary Table 1. Experiments at site RI stretch over several years and are aggregated to the annual level in panel (b) of Figure 6. The dry experiments generally show k_{sat} values 2–3 times higher than the wet experiments. When comparing the calibrated k_{sat} values for every two associated experiments without aggregating them further, each pair shows higher k_{sat} for the dry than for the wet experiment.

3.2.4 | Cohesion COH for all sites versus literature and measured values

Figure 7a provides the calibrated COH values compared with data from Morgan et al. (1998) and torvane measurements for group A experiments. The COH values for the remaining sites where no torvane measurements are available are shown in Figure 7b. There is good agreement at the lower end of the COH range for sites SOMO, STRA, RIT4, RIT5. Sites RI17, RI18, NAGY AN11, AN12 and ROTT show some agreement, while sites RI19, RI16, RIVA, TETF and RIT6 do not seem to fit together. Some agreement exists between measured and calibrated values for sites ROTT and NAGY, where the interquartile ranges overlap. The measurements for the remaining sites RIT6, TETF, RIVA, RIT5, RIT4 and SOMO do neither agree with the calibrated values nor with the ranges from Morgan et al. (1998). Measured values are larger than 12 kPa, the maximum value for COH suggested by Morgan (2001) at sites TETF, RIVA and SOMO.

3.2.5 | Concentration factor C_F for all sites

The calibrated values for parameter C_F are shown in Figure 8, with about half of the sites ranging close to values of around 1–2. The highest values were attained for sites SOMO and RI16-19, and moderately high values were received at sites RIVA, TETF, and STRA.

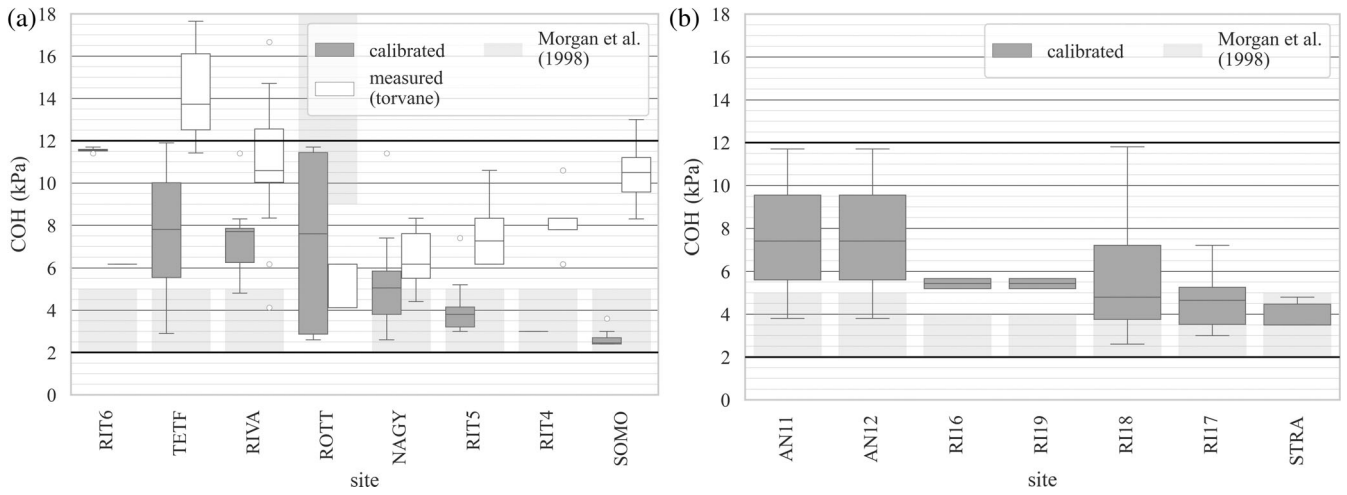

FIGURE 7 COH values calibrated with the CASE model for all rainfall experiments grouped by site (grey boxplots, 'calibrated'); light grey shaded boxes are the ranges for COH given in Morgan et al. (1998); measured COH values (white boxplots) are only available for experiments from group A; COH values between 2 and 12 were the range used in calibration/validation; each data point represents one experiment; y-axis cut off at 18 kPa.

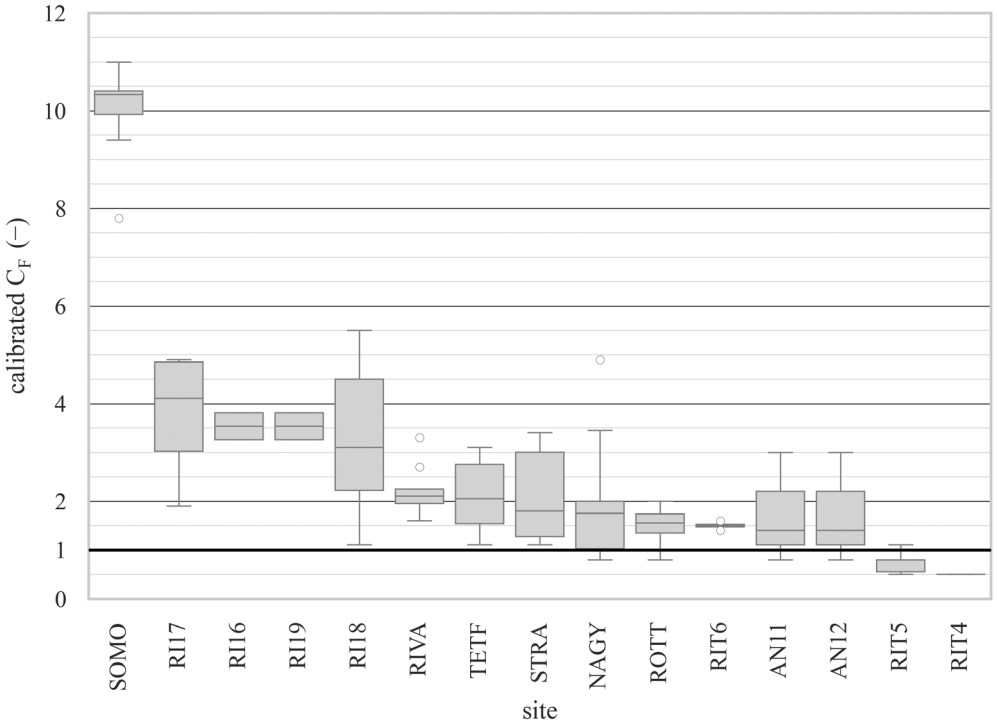

FIGURE 8 C_F values calibrated with the CASE model for all rainfall experiments grouped per site; solid black line represents the default value of $C_F = 1$.

4 | DISCUSSION

4.1 | Sensitivity analysis

We identified three studies using models from the MMF family that performed a dedicated sensitivity analysis for all model parameters. While Morgan and Duzant (2008) and Jain and Ramsankaran (2018) used the ALS index for rating the parameter sensitivities as we did, Choi et al. (2017) used Sobol' total indices as described by Sobol' (2001). To contrast the different results, we only used those equivalent to the parameters used in our study. Table 4 provides a comparison of the different sensitivities that were obtained.

Not surprisingly, the sensitivity of the parameters controlling splash (K/RD/DK) and runoff detachment (COH/OD/DR) show high variability among the different studies since different spatial scales were considered. The size of the study area is presumably the dominant factor in the relative importance of splash or runoff detachment due to surface runoff accumulation following a nonlinear increase in typical landscapes. Similarly, CC (affecting only splash detachment) and GC (affecting only runoff detachment) show high variability too.

TABLE 4 Comparison of parameter sensitivities for different studies of the Morgan-Morgan-Finney model family.

	Parameter sensitivity				
	Spatial scale				
	CASE	Morgan and Duzant (2008)[a]	Jain and Ramsankaran (2018)[b]	Choi et al. (2017)[c]	
Parameter	Plot	Element	Catchment	Field	Element
swc_{sat}/θ_{sat}[c]	++	n/a	n/a	+	++
swc_{init}/θ_{init}[c]	++	n/a	n/a	n/a	++
k_{sat}/K[c]	++	n/a	n/a	+	o
G	++	n/a	n/a	n/a	n/a
C_F	++	n/a	n/a	n/a	n/a
K[b]/RD[a]/DK[c]	+	++	o	o	o
C	+	n/a	+	n/a	n/a
CC	+	++	++	n/a	o
GC	o	o	++	o	+
PH	o	+	o	n/a	o
A/PI[a,b,c]	+	o	o	o	+
COH/OD[a]/DR[b,c]	o	o	+	++	o

Note: '++' = high sensitivity, '+' = moderate sensitivity and 'o' = low sensitivity; sensitivities are rated as absolute values; detailed parameter definitions may be looked up in the respective studies. Superscripts [a, b, c] indicate parameter abbreviations as used by different studies, the first parameter abbreviation in each row is that used in the CASE model; remaining non-comparable parameters are not included.

Parameters A/PI and PH show mostly low sensitivities, which might be a reason to doubt the value added by these parameters (Table 5).

From Table 4, we may deduce that even though all studies deal with a similar modelling approach, the parameter sensitivities may differ considerably. It is also interesting to see that K (k_{sat}) sensitivity even varies within the same study when changing the spatial scale from a single element to a field (Choi et al., 2017). The differences in parameter sensitivities between these studies are supposedly due to different characteristics and experimental setups within the input data that were not varied in the sensitivity analysis. Even when comparing the sensitivities for the same model, individual parameter sensitivities might vary substantially for comparatively homogeneous datasets, as shown by the distributions of our ALS values for the CASE model in Figure 3. Thus, we suggest that the merit of directly comparing different sensitivity indicators for different models with different datasets remains limited. An analysis following the framework described by Cheviron et al. (2010) would be more appropriate (different models applied to the same virtual catchment) but out of scope for this study. However, it allows for basic statements about the conceptual validity of parameter relations to output (e.g., increased runoff with decreased k_{sat}). These general process mechanics and parameter relationships are lined out in hydrological and soil erosion textbooks like Morgan (2005) or Beven (2012).

4.2 | Saturated hydraulic conductivity k_{sat}

The calibrated k_{sat} values generally show satisfactory agreement with k_{sat} values calculated by a range of 14 different PTFs, as shown in Figure 5. Differences are small given the high spatial and temporal variability and problems typically involved in the measurement and upscaling of this parameter, see, for example, Picciafuoco et al. (2019a), Alletto and Coquet (2009) or Baiamonte et al. (2017). The selection of the PTFs was guided by data availability and closely followed a compilation of PTFs given by Abdelbaki et al. (2009). These are probably somewhat biased towards US soils. We tried to balance this by introducing the PTFs from Szabó et al. (2021) with a clear focus on European conditions. The performance of these PTFs in predicting the k_{sat} values calibrated with the CASE model is shown in Table 3. One of the two error measures we used is the mean relative error (MRE), which allows rating a general tendency of under- or overestimation. Both evaluation criteria were selected following Nasta et al. (2021). The three PTFs labelled KS01, KS03 and KS05 in Table 3 show the lowest RMSE and MRE values in predicting the calibrated k_{sat} values, which leads us to recommend their use. Some of the more straightforward PTFs, that is, Puckett et al. (1985), Ferrer Julià et al. (2004) and Weynants et al. (2009), show small error values as well and can be recommended.

Moreover, calibrated k_{sat} values were shown to behave as expected for two special cases that are covered by our dataset: decreasing k_{sat} with repeatedly applied rainfall and experiments with varying initial soil moisture states ('dry' and 'wet'). Concerning repeated rainfall, one would expect decreasing k_{sat} values with each additional rainfall applied due to increased aggregate disintegration and surface sealing. Panel (a) of Figure 6 shows that this is the case for most of the experiments from group A. Similar behaviour was found with rainfall experiments, for example, by Zambon et al. (2021) and Bedaiwy (2008). Fiener, Auerswald, and

TABLE 5 Site characteristics of the rainfall experiments contained in the dataset.

Site	Hungary		Italy		Austria					Czech Republic
Characteristics	Nagyhorváti	Somogybabod	Riva	Tetto Frati	Ritzlhof		Rottenhaus	Stranzendorf	Antiesen	Risuty
Short name	NAGY	SOMO	RIVA	TETF	RIT4	RIT5,6	ROTT	STRA	AN11, 12	RI16, 17, 18,19
Coordinates (EPSG: 4326)	46°41′27.9″ N 17°05′13.3″ E	46°40′22.1″ N 17°44′43.8″ E	44°58′41.3″ N 7°53′19.8″ E	44°53′16.7″ N 7°41′12.4″ E	48°11′03.8″ N 14°14′52.5″ E		48°07′00.5″N 15°09′01.9″ E	48°26′32.4″ N 16°04′10.7″ E	48°19′35.7″ N 13°28′43.34″ E	50°13′01.2″ N 14°01′01.2″ E
Mean annual rainfall sum (mm)	687	751	755		753		744	500	1051	690
Mean annual temperature (°)	11.6		12.0		8.8		9.1	8.8	7.8	8.7
Soil type (WRB)	Haplic luvisol	Calcaric regosol	Eutric fluvisol		Dystric cambisol		Stagni-calcaric cambisol	Dystric planosol	Humic gleysol	Loamic cambisol
Topsoil particle size fractions (% sand/silt/clay)	30/50/20	27/56/17	11/69/20	27/61/12	17/60/23	16/61/23	7/60/33	17/70/13	11/21/68	46/19/35
TOC content (%)	1.0	0.9	0.9	1.1	1.3	1.7	1.6	0.6	1.3	1.2
Slope (°)	7.5	13.0	0.3	0.3	8.0	8.1	15.0–18.0	10.0	7.9	5.1
Experiment group	A	A	A	A	A	A	A	B	C	D

Van Oost (2011) note that several studies model the reduction in infiltration rate due to sealing using negative exponential equations that commonly depend on either total rainfall or rainfall kinetic energy. Zambon et al. (2021) investigated the effect using rainfall experiments on splash cups and derived regressions for k_{sat} depending on the accumulated kinetic energy of rainfall for specific soils.

Concerning different initial soil moisture states for the experiments of group D, as shown in panel (b) of Figure 6, lower k_{sat} values with higher values of swc_{init} are the necessary outcome when calculating infiltration according to Smith and Parlange (1978) and Woolhiser et al. (1990), as it happens in the CASE water phase.

4.3 | COH

Direct use of the topsoil cohesion, or its reciprocal value as resistance (Equation 8), appears to be limited to the MMF model family and the EUROSEM model. Other models mostly rely either on more empirical runoff erodibility values (similar to the rainfall erodibility K in MMF models) or on hydraulic calculations based on some critical shear resistance of the soil that the runoff might exceed. For example, the WEPP model uses interrill erodibility, rill erodibility and critical shear (Flanagan & Livingston, 1995). Tan et al. (2018) interpreted the differentiation between K (only affecting splash detachment) and COH (only affecting runoff detachment) in the MMF model family, as a valid way to differentiate between rill (=runoff detachment) and interrill (=splash detachment) erosion. Peñuela et al. (2017), (2018) pointed out an error in the calculation of KE(LD) that has propagated through several MMF model versions and propose a corrected and expanded method of differentiation between rainfall and runoff detachment in their MMF-TWI model. Only when actual discrete runoff volumes per timestep can be calculated satisfactorily, as is done in models relying on the critical shear stress concept, it seems reasonable to use this approach. The runoff calculations in all MMF models are temporally lumped, for example, in the CASE model, only the total event runoff is provided. Therefore some degree of empiricism when applying the MMF model family is unavoidable.

Morgan (2001) suggests measurement of the parameter COH using a torvane shear device, which is a standard measurement technique in geotechnical engineering but has also been used with soil erosion, for example, by Zimbone et al. (1996), Vigiak et al. (2005), and Torri and Poesen (2014). For that part of our dataset (experiments of group A), where replicated torvane measurements are available, they show poor agreement with the COH values calibrated with the CASE model and values for COH taken from Morgan et al. (1998), as shown in Figure 7a. This is also supported by the findings of Léonard and Richard (2004), who state the difficulty in deriving measured values for COH. Also, Morgan et al. (1998) note the difficulty involved in performing direct measurements of COH especially when plant roots are present and suggest adjustments of COH for various types of vegetation. Mainly because of the known difficulties around directly measuring the parameter, it was used for calibration in this

study – instead of relying on the measured values that are available at least for part of the dataset. COH shows only low sensitivity in the CASE model (Figure 3).

For these reasons, we suggest considering the parameters in the different models as 'effective parameters' based on physical considerations rather than directly measurable physical properties, as Beven (2012) discussed.

4.4 | Concentration factor C_F

Results for the calibrated C_F parameter show the highest values for sites SOMO and RI, which both have Loess as the parent material. The results suggest that the default value of 1 would be an acceptable estimate for most cases we investigated. Changing the value of C_F would thus be justified for two reasons: (1) for comparison with measured data, (2) when the parent material of a site is Loess, or it is especially prone to rill formation. Other studies employed similar modifications to the runoff or transport capacity calculations as we made by introducing the parameter C_F. Prosser and Rustomji (2004) give an overview of sediment transport capacity relations for overland flow, some of which are formulated similarly to the transport capacity relation from Morgan (2001) (Equation 3). Wang et al. (2019) categorize this type of transport capacity calculation as empirical. It has to be noted that Q calculated in our model represents the lumped cumulative runoff at the end of the event and, therefore, cannot directly be used in hydraulic calculations like instantaneous runoff—this is even more true for the temporally much coarser Q calculated by Morgan (2001). This is why the exponents used for H and Q in Equations (3) and (9) have a somewhat arbitrary character in our context. Sterk (2021), for example, used this exponent in the TC calculation as a calibration factor. During calibration of the model, it became clear that it could not reproduce some of the highest measured soil loss rates in the dataset of this study using the default H calculation from Morgan (2001), while the lower or medium rates did not pose a problem. Some reference to this issue can also be found in Renard et al. (1997), where it is addressed with modifying the RUSLE LS factor according to rill/interrill erosion classes.

Results for the different parameters were mixed: Calibrated k_{sat} values appear behavioural, and the estimation of k_{sat} employing PTF proved unproblematic. For the sediment phase on the other hand, calibrated parameter values for COH showed poor agreement with both literature values and measurements, while the introduction of a new parameter C_F was necessary for the model to reproduce some of the highest measured soil loss values in the dataset.

4.5 | Infiltration excess runoff assumption

There has been an ongoing debate about the relative significance of infiltration excess ('Hortonian') and saturation excess (Cappus, 1960; Dunne & Black, 1970) as the dominant process of overland flow generation within a catchment, see for example, Beven (2012) and Beven (2021), who gives an extensive account of how these concepts evolved over time. According to Beven (2021), this has been going on since the very early days of hydrology as a science. Scientific advancements in recent decades (e.g., geochemical and isotope hydrograph separation) have quite clearly shown that in many catchments, displacement of pre-event water plays an important role. At the catchment scale, overland flow resulting exclusively from infiltration excess seems to be a rather rare event under many circumstances. Presumably, the relative importance of the two mechanisms varies for each specific catchment and with each individual rainfall event (with different initial conditions, antecedent soil moisture state, etc.). In the end, overland flow will typically be the result of a combination of the two mechanisms. These catchment hydrological considerations do not share our focus on sediment detachment and transport, which is why they seem of limited applicability. Apart from that, the debate does not seem to have concluded to choose one concept over the other but favouring their combination whenever possible. We are aware that our limitation to infiltration excess surface runoff is a simplification, yet we are implementing a model to simulate soil erosion for high-intensity (=erosive) rainfall events, and not catchment hydrology and runoff per se. Given these considerations, we regard our arbitrary model choice as justified. Entekhabi and Eagleson (1989) investigated the relative importance of infiltration excess ('Hortonian' in their work) and saturation excess runoff ('Dunne' in their work). While the ratios of infiltration rate to precipitation intensity ('I' in their work) were usually above 1 in their study, a ratio of $I = k_{sat}/I$ (k_{sat} and right hand I from CASE) is in our dataset at a maximum of around 1 (one site), but usually well below 1 and even <0.1. Entekhabi and Eagleson (1989) do not cover these parameter combinations, but an extrapolation of their Figure 2 suggests the increased importance of infiltration excess runoff with $I < 1$. The calculated values of I for our dataset are contained in Supplementary Table 1, labelled I_{diff} using the difference between total measured runoff and applied amount of rainfall, and I_{ksat} using our calibrated k_{sat} values.

5 | CONCLUSIONS AND OUTLOOK

In this study, changes to an erosion model based on the RMMF and MMMF models are proposed to enable the calculation of runoff and soil loss for individual rainfall events. The model was calibrated and validated with a dataset consisting of 142 high-intensity rainfall experiments on bare soil plots. For climatic conditions in Central Europe, the information about soil loss during periods of high rainfall intensities and low soil or canopy cover is of high interest. This usually refers to the spring period with single heavy rainstorms occurring immediately after seedbed preparation and seeding of summer crops. These considerations are reflected in our choice of data set and the model we employed. The model reproduced the measured runoff

volumes and soil loss masses observed during the experiments with a satisfactory agreement.

Results for the plausibility of the different calibrated parameters were mixed: k_{sat} values appear behavioural, and the estimation of k_{sat} employing PTF suggests that our values lie within a plausible range of results. For the sediment phase, on the other hand, calibrated parameter values for COH showed poor agreement with both literature values and measurements, and the introduction of a new parameter C_F was necessary for the model to reproduce some of the highest measured soil loss values in the dataset.

Our results also demonstrate that different experiment preconditions, such as repeated rainfall or soil wetness, are logically reflected in the parameter values of our model. This provides confidence that the calibrated parameter values may be helpful in further model applications for the validated conditions and may give some guidance for similar conditions.

The results of our procedure are limited to the soil conditions after seedbed preparation and seeding until a sufficient soil cover has developed. Along with the higher procedural detail associated with the introduction of an infiltration model into the water phase of the model comes an increased dependence on parameters that are difficult to measure or predict (especially k_{sat} and swc_{init}). Also, additional inputs like soil water balance would be needed to apply the model in real-world settings with more than one event. In its current state, the model has do be considered a model for research purposes (parameter calibration, scenario comparison) and not a model to be applied, for example, by farmers or the general public.

ACKNOWLEDGEMENTS

We would like to acknowledge the provision of rainfall experiment data from the Federal Agency for Water Management, Institute for Soil and Water Management Research, Petzenkirchen, Austria, Czech Technical University, Prague, Czech Republic, University of Pannonia, Georgikon Faculty of Agriculture, Keszthely, Hungary and University of Torino, Department of Agricultural, Forest and Food Sciences, Grugliasco, Italy. Part of these simulations were performed using funding from the EU financed project 'DESPRAL – An environmental soil test to determine the potential from Sediment and Phosphorous transfer in Run-off from Agricultural Land', contract number EVK1-CT-1999-00007. Funding for this work was also obtained within the EU financed projects 'Soil Hydrology research platform underpinning innovation to manage water scarcity in European and Chinese cropping systems – SHui' (Grant No. 773903) and 'Transforming Unsustainable management of soils in key agricultural systems in EU and China – TUdi' (Grant No. 101000224), for which we are grateful.

CONFLICT OF INTEREST STATEMENT

The authors declare no conflicts of interest.

DATA AVAILABILITY STATEMENT

The data that support the findings of this study are available from the corresponding author upon reasonable request.

ORCID

Thomas Brunner https://orcid.org/0000-0002-0402-219X
Thomas Weninger https://orcid.org/0000-0001-9004-4426
Elmar Schmaltz https://orcid.org/0000-0003-4016-2891
Josef Krasa https://orcid.org/0000-0003-4067-5806
Jakub Stasek https://orcid.org/0000-0001-9313-8946
Laura Zavattaro https://orcid.org/0000-0001-8199-7399
Istvan Sisak https://orcid.org/0000-0001-9138-7068
Tomas Dostal https://orcid.org/0000-0003-3984-3462
Andreas Klik https://orcid.org/0000-0002-3299-1721
Peter Strauss https://orcid.org/0000-0002-8693-9304

REFERENCES

Abdelbaki, A. M., Youssef, M. A., Naguib, E. M. F., Kiwan, M. E., & El-giddawy, E. I. (2009). Evaluation of Pedotransfer functions for predicting saturated hydraulic conductivity for U.S. soils. *American Society of Agricultural and Biological Engineers Annual International Meeting 2009, ASABE 2009*, *10*(1), 6583–6602.

Alder, S., Prasuhn, V., Liniger, H., Herweg, K., Hurni, H., Candinas, A., & Gujer, H. U. (2015). A high-resolution map of direct and indirect connectivity of erosion risk areas to surface waters in Switzerland-a risk assessment tool for planning and policy-making. *Land Use Policy*, *48*, 236–249. https://doi.org/10.1016/j.landusepol.2015.06.001

Alletto, L., & Coquet, Y. (2009). Temporal and spatial variability of soil bulk density and near-saturated hydraulic conductivity under two contrasted tillage management systems. *Geoderma*, *152*(1–2), 85–94. https://doi.org/10.1016/j.geoderma.2009.05.023

Antoine, M., Javaux, M., & Bielders, C. (2009). What indicators can capture runoff-relevant connectivity properties of the micro-topography at the plot scale? *Advances in Water Resources*, *32*(8), 1297–1310. https://doi.org/10.1016/j.advwatres.2009.05.006

Appels, W. M., Bogaart, P. W., & van der Zee, S. E. (2011). Influence of spatial variations of microtopography and infiltration on surface runoff and field scale hydrological connectivity. *Advances in Water Resources*, *34*(2), 303–313. https://doi.org/10.1016/j.advwatres.2010.12.003

Auerswald, K., Kainz, M., & Fiener, P. (2003). Soil erosion potential of organic versus conventional farming evaluated by USLE modelling of cropping statistics for agricultural districts in Bavaria. *Soil Use and Management*, *19*(4), 305–311.

Baiamonte, G., Bagarello, V., D'Asaro, F., & Palmeri, V. (2017). Factors influencing point measurement of near-surface saturated soil hydraulic conductivity in a small Sicilian Basin. *Land Degradation and Development*, *28*(3), 970–982.

Batista, P. V. G., Davies, J., Silva, M. L. N., & Quinton, J. N. (2019). On the evaluation of soil erosion models: Are we doing enough? *Earth-Science Reviews*, *197*(5), 102898. https://doi.org/10.1016/j.earscirev.2019.102898

Bedaiwy, M. N. A. (2008). Mechanical and hydraulic resistance relations in crust-topped soils. *Catena*, *72*(2), 270–281.

Beven, K. J. (2006). A manifesto for the equifinality thesis. *Journal of Hydrology*, *320*(1–2), 18–36.

Beven, K. J. (2012). Rainfall-runoff modelling.

Beven, K. J. (2021). The era of infiltration. *Hydrology and Earth System Sciences*, *25*(2), 851–866.

Beven, K. J., & Binley, A. (1992). The future of distributed models: Model calibration and uncertainty prediction. *Hydrological Process*, *6*, 298.

Bezak, N., Mikoš, M., Borrelli, P., Alewell, C., Alvarez, P., Anache, J. A. A., Baartman, J., Ballabio, C., Biddoccu, M., Cerdà, A., Chalise, D., Chen, S., Chen, W., De Girolamo, A. M., Gessesse, G. D., Deumlich, D., Diodato, N., Efthimiou, N., Erpul, G., … Panagos, P. (2021). Soil erosion modelling: A bibliometric analysis. *Environmental Research*, *197*(3), 111087.

Blasone, R. S., Vrugt, J. A., Madsen, H., Rosbjerg, D., Robinson, B. A., & Zyvoloski, G. A. (2008). Generalized likelihood uncertainty estimation (GLUE) using adaptive Markov chain Monte Carlo sampling. *Advances in Water Resources*, *31*(4), 630–648.

Boardman, J. (2006). Soil erosion science: Reflections on the limitations of current approaches. *Catena*, *68*(2–3), 73–86.

Brakensiek, D. L., Rawls, W. J., & Stephenson, G. R. (1984). ASAE paper no. PNR-84203 modifying SCS hydrologic soil groups and curve numbers for rangeland soils.

Brazier, R. E., Beven, K. J., Anthony, S. G., & Rowan, J. S. (2001). Implications of model uncertainty for the mapping of hillslope-scale soil erosion predictions. *Earth Surface Processes and Landforms*, *26*(12), 1333–1352.

Brazier, R. E., Beven, K. J., Freer, J., & Rowan, J. S. (2000). Equifinality and uncertainty in physically based soil erosion models: Application of the Glue methodology to Wepp-the water erosion prediction project-for sites in the UK and USA. *Earth Surface Processes and Landforms*, *25*(8), 825–845.

Cappus, P. (1960). Étude Des Lois De L'Écoulement–Application Au Calcul Et Aà La Prévision Des Débits. *Houille Blanche*, *46*, 493–520.

Cea, L., Legout, C., Grangeon, T., & Nord, G. (2016). Impact of model simplifications on soil erosion predictions: Application of the GLUE methodology to a distributed event-based model at the hillslope scale. *Hydrological Processes*, *30*(7), 1096–1113.

Cheviron, B., Gumiere, S. J., Le Bissonnais, Y., Moussa, R., & Raclot, D. (2010). Sensitivity analysis of distributed erosion models: Framework. *Water Resources Research*, *46*(8). https://doi.org/10.1029/2009wr007950

Choi, K., Arnhold, S., Huwe, B., & Reineking, B. (2017). Daily based Morgan-Morgan-Finney (Dmmf) model: A spatially distributed conceptual soil erosion model to simulate complex soil surface configurations. *Water (Switzerland)*, *9*(4), 278.

Cosby, B. J., Hornberger, G. M., Clapp, R. B., & Ginn, T. R. (1984). A statistical exploration of the relationships of soil moisture characteristics to the physical properties of soils. *Water Resources Research*, *20*(6), 682–690.

Dane, J. H., & Puckett, W. E. (1994). Field soil hydraulic properties based on physical and minerological information. In M. T. Van Genuchten (Ed.), *Proceedings of the international workshop on indirect methods for estimating the hydraulic properties of unsaturated soils* (pp. 317–328). University of California.

de Vente, J., & Poesen, J. (2005). Predicting soil erosion and sediment yield at the basin scale: Scale issues and semi-quantitative models. *Earth-Science Reviews*, *71*(1–2), 95–125.

Dunne, T., & Black, R. D. (1970). An experimental investigation of runoff production in permeable soils. *Water Resources Research*, *6*(2), 478–490.

Edwards, W. M., & Owens, L. B. (1991). Large storm effects on total soil erosion. *Journal of Soil and Water Conservation*, *46*, 78.

Eekhout, J. P. C., Terink, W., & De Vente, J. (2018). Assessing the large-scale impacts of environmental change using a coupled hydrology and soil erosion model. *Earth Surface Dynamics*, *6*(3), 687–703.

Entekhabi, D., & Eagleson, P. S. (1989). Land surface hydrology parameterization for atmospheric general circulation models including subgrid scale spatial variability. *Journal of Climate*, *2*(8), 816–831.

Feng, T., Chen, H., Wang, K., Zhang, W., & Qi, X. (2014). Modeling soil erosion using a spatially distributed model in a karst catchment of Northwest Guangxi, China. *Earth Surface Processes and Landforms*, *39*(15), 2121–2130.

Ferrer Julià, M., Estrela Monreal, T., Jiménez, A. S. D. C., & Meléndez, E. G. (2004). Constructing a saturated hydraulic conductivity map of Spain using pedotransfer functions and spatial prediction. *Geoderma*, *123*(3–4), 257–277.

Fiener, P., Auerswald, K., & Van Oost, K. (2011). Spatio-temporal patterns in land use and management affecting surface runoff response of agricultural catchments-a review. *Earth-Science Reviews*, *106*(1–2), 92–104. https://doi.org/10.1016/j.earscirev.2011.01.004

Fiener, P., Seibert, S. P., & Auerswald, K. (2011). A compilation and meta-analysis of rainfall simulation data on arable soils. *Journal of Hydrology*, *409*(1–2), 395–406. https://doi.org/10.1016/j.jhydrol.2011.08.034

Flanagan, D. C., & Livingston, S. J. (1995). WEPP user summary. Vol. 11, pp. 141.

Gassman, P. W., Reyes, M. R., Green, C. H., & Arnold, J. G. (2007). The soil and water assessment tool: Historical development, applications, and future research directions. *Transactions of the ASABE*, *50*(4), 1211–1250.

Gonzalez-Hidalgo, J. C., Batalla, R. J., Cerda, A., & de Luis, M. (2012). A regional analysis of the effects of largest events on soil erosion. *Catena*, *95*, 85–90. https://doi.org/10.1016/j.catena.2012.03.006

González-Hidalgo, J. C., de Luis, M., & Batalla, R. J. (2009). Effects of the largest daily events on total soil erosion by rainwater. An analysis of the USLE database. *Earth Surface Processes and Landforms*, *34*(15), 2070–2077. https://doi.org/10.1002/esp.1892

Govers, G. (2010). Misapplications and misconceptions of erosion models. *Handbook of Erosion Modelling*, 117–134. Portico. https://doi.org/10.1002/9781444328455.ch7

Govers, G., Takken, I., Helming, K., Govers, G., Takken, I., & Helming, K. (2000). Soil roughness and overland flow. *Agronomie*, *20*(2), 131–146.

Hengl, T., Mendes de Jesus, J., Heuvelink, G. B. M., Ruiperez Gonzalez, M., Kilibarda, M., Blagotić, A., Shangguan, W., Wright, M. N., Geng, X., Bauer-Marschallinger, B., Guevara, M. A., Vargas, R., MacMillan, R. A., Batjes, N. H., Leenaars, J. G. B., Ribeiro, E., Wheeler, I., Mantel, S., & Kempen, B. (2017). SoilGrids250m: Global gridded soil information based on machine learning. *PLOS ONE*, *12*(2), e0169748. https://doi.org/10.1371/journal.pone.0169748

Hollis, J. M., Lilly, A., Higgins, A., Jones, R. J. A., Keay, C. A., & Bellamy, P. (2015). Predicting the water retention characteristics of UK mineral soils. *European Journal of Soil Science*, *66*(1), 239–252.

Hösl, R., & Strauss, P. (2016). Conservation tillage practices in the alpine forelands of Austria–are they effective? *Catena*, *137*, 44–51. https://doi.org/10.1016/j.catena.2015.08.009

Hu, W., She, D., Shao, M.'a., Chun, K. P., & Si, B. (2015). Effects of initial soil water content and saturated hydraulic conductivity variability on small watershed runoff simulation using LISEM. *Hydrological Sciences Journal*, *60*(6), 1137–1154. https://doi.org/10.1080/02626667.2014.903332

Jabro, J. D. (1992). Estimation of saturated hydraulic conductivity of soils from particle size distribution and bulk density data. *Transactions of the ASAE*, *35*(2), 557–560.

Jain, P., & Ramsankaran, R. A. A. J. (2018). GIS-based modelling of soil erosion processes using the modified-MMF (MMMF) model in a large watershed having vast Agro-climatological differences. *Earth Surface Processes and Landforms*, *43*(10), 2064–2076.

Jenson, S. K., & Dominque, J. O. (1988). Extracting topographic structure from digital elevation data for geographic information system analysis. *Photogrammetric Engineering and Remote Sensing*, *54*(11), 1593–1600.

Jetten, V., Govers, G., & Hessel, R. (2003). Erosion models: Quality of spatial predictions. *Hydrological Processes*, *17*(5), 887–900.

Johannsen, L. L., Schmaltz, E., Mitrovits, O., Klik, A., Smoliner, W., Wang, S., & Strauss, P. (2022). An update of the spatial and temporal variability of rainfall erosivity (R-factor) for the Main agricultural production zones of Austria. *Catena*, *215*(3), 1–14.

Johannsen, L. L., Zambon, N., Strauss, P., Dostal, T., Neumann, M., Zumr, D., Cochrane, T. A., & Klik, A. (2020). Impact of disdrometer types on rainfall erosivity estimation. *Water*, *12*(4), 963. https://doi.org/10.3390/w12040963

Kavka, P., Dostál, T., Iserloh, T., Davidová, T., Josef Krása, V., David, J. V., Khel, T., & Bauer, M. (2015). A medium scale Mobile rainfall simulator for experiments on soil erosion and soil hydrology. *Geophysical Research Abstracts*, *17*(1), 330118.

Kinnell, P. I. A. (2010). Event soil loss, runoff and the universal soil loss equation family of models: A review. *Journal of Hydrology*, *385*(1–4), 384–397. https://doi.org/10.1016/j.jhydrol.2010.01.024

Kinnell, P. I. A. (2016). A review of the design and operation of runoff and soil loss plots. *Catena*, *145*, 257–265. https://doi.org/10.1016/j.catena.2016.06.013

Kinnell, P. I. A. (2017). A comparison of the abilities of the USLE-M, RUSLE2 and WEPP to model event erosion from bare fallow areas. *Science of the Total Environment*, *596–597*, 32–42. https://doi.org/10.1016/j.scitotenv.2017.04.046

Kinnell, P. I. A., & Risse, L. M. (1998). USLE-M: Empirical modeling rainfall erosion through runoff and sediment concentration. *Soil Science Society of America Journal*, *62*(6), 1667–1672.

Klik, A., & Eitzinger, J. (2010). Impact of climate change on soil erosion and the efficiency of soil conservation practices in Austria. *Journal of Agricultural Science*, *148*(5), 529–541.

Lannoy, D., Gabriëlle, J. M., Verhoest, N. E. C., Houser, P. R., Gish, T. J., & van Meirvenne, M. (2006). Spatial and temporal characteristics of soil moisture in an intensively monitored agricultural field (OPE3). *Journal of Hydrology*, *331*(3–4), 719–730.

Lawrence, D. S. L. (1997). Macroscale surface roughness and frictional resistance in overland flow. *Earth Surface Processes and Landforms*, *22*(4), 365–382.

Léonard, J., & Richard, G. (2004). Estimation of runoff critical shear stress for soil erosion from soil shear strength. *Catena*, *57*(3), 233–249.

Li, C., Qi, J., Feng, Z., Yin, R., Guo, B., Zhang, F., & Zou, S. (2010). Quantifying the effect of ecological restoration on soil erosion in China's loess plateau region: An application of the MMF approach. *Environmental Management*, *45*(3), 476–487.

Li, Y., Chen, D., White, R. E., Zhu, A., & Zhang, J. (2007). Estimating soil hydraulic properties of Fengqiu County soils in the North China plain using pedo-transfer functions. *Geoderma*, *138*(3–4), 261–271.

Lilhare, R., Garg, V., & Nikam, B. R. (2015). Application of GIS-coupled modified MMF model to estimate sediment yield on a watershed scale. *Journal of Hydrologic Engineering*, *20*(6), C5014002.

López-Vicente, M., Navas, A., & Machín, J. (2008). Modelling soil detachment rates in rainfed agrosystems in the South-Central Pyrenees. *Agricultural Water Management*, *95*(9), 1079–1089.

Luo, J., Zheng, Z., Li, T., & He, S. (2020). Catena spatial variation of microtopography and its effect on temporal evolution of soil erosion during different erosive stages. *Catena*, *190*(2), 104515. https://doi.org/10.1016/j.catena.2020.104515

Mirzaei, M., Huang, Y. F., El-Shafie, A., & Shatirah, A. (2015). Application of the generalized likelihood uncertainty estimation (GLUE) approach for assessing uncertainty in hydrological models: A review. *Stochastic Environmental Research and Risk Assessment*, *29*(5), 1265–1273. https://doi.org/10.1007/s00477-014-1000-6

Morgan, R. P. C. (2001). A simple approach to soil loss prediction: A revised Morgan-Morgan-Finney model. *Catena*, *44*(4), 305–322.

Morgan, R. P. C. (2005). *Soil erosion and conservation* (3rd ed.). Blackwell Publishing.

Morgan, R. P. C., & Duzant, J. H. (2008). Modified MMF (Morgan–Morgan–Finney) model for evaluating effects of crops and vegetation cover on soil erosion. *Earth Surface Processes and Landforms*, *33*(1), 90–106.

Morgan, R. P. C., Morgan, D. D. V., & Finney, H. J. (1984). A predictive model for the assessment of soil erosion risk. *Journal of Agricultural Engineering Research*, *30*, 245–253.

Morgan, R. P. C., Quinton, J. N., Smith, R. E., Govers, G., Poesen, J., Auerswald, K., Chisci, G., Torri, D., Styczen, M. E., & Folly, A. J. V. (1998). *The European soil erosion model (EUROSEM): Documentation and user guide, version 3.6*. Silsoe College, Cranfield University.

Nasta, P., Szabó, B., & Romano, N. (2021). Evaluation of Pedotransfer functions for predicting soil hydraulic properties: A voyage from regional to field scales across Europe. *Journal of Hydrology: Regional Studies*, *37*(2), 100903.

Nearing, M. A. (1998). Why soil erosion models over-predict small soil losses and under-predict large soil losses. *Catena*, *32*(1), 15–22.

Nearing, M. A. (2000). Evaluating soil erosion models using measured plot data: Accounting for variability in the data. *Earth Surface Processes and Landforms*, *25*, 1035–1043.

Nearing, M. A., Deer-Ascough, L., & Laflen, J. M. (1990). Sensitivity analysis of the WEPP hillslope profile erosion model. *Transactions of the American Society of Agricultural Engineers*, *33*(3), 839–849.

Oost, V., Kristof, G. G., & Desmet, P. (2000). Evaluating the effects of changes in landscape structure on soil erosion by water and tillage. *Landscape Ecology*, *15*(6), 577–589.

Panagos, P., Borrelli, P., Spinoni, J., Ballabio, C., Meusburger, K., Beguería, S., Klik, A., Michaelides, S., Petan, S., Hrabalíková, M., Olsen, P., Aalto, J., Lakatos, M., Rymszewicz, A., Dumitrescu, A., Perčec Tadić, M., Diodato, N., Kostalova, J., Rousseva, S., … Alewell, C. (2016). Monthly rainfall erosivity: Conversion factors for different time resolutions and regional assessments. *Water*, *8*(4), 119. https://doi.org/10.3390/w8040119

Pandey, A., Mathur, A., Mishra, S. K., & Mal, B. C. (2009). Soil erosion modeling of a Himalayan watershed using RS and GIS. *Environmental Earth Sciences*, *59*(2), 399–410.

Patil, N. G., & Singh, S. K. (2016). Pedotransfer functions for estimating soil hydraulic properties: A review. *Pedosphere*, *26*(4), 417–430.

Peñuela, A., Javaux, M., & Bielders, C. L. (2013). Scale effect on overland flow connectivity at the plot scale. *Hydrology and Earth System Sciences*, *17*(1), 87–101.

Peñuela, A., Sellami, H., & Smith, H. G. (2017). Modelling catchment soil erosion: A critique of Morgan-Morgan-Finney model and a revised approach. *Geophysical Research Abstracts*, *19*, 5282.

Peñuela, A., Sellami, H., & Smith, H. G. (2018). A model for catchment soil erosion management in humid agricultural environments. *Earth Surface Processes and Landforms*, *43*(3), 608–622.

Perrin, C., Michel, C., & Andréassian, V. (2001). Does a large number of parameters enhance model performance? Comparative assessment of common catchment model structures on 429 catchments. *Journal of Hydrology*, *242*(3), 275–301.

Picciafuoco, T., Morbidelli, R., Flammini, A., Saltalippi, C., Corradini, C., Strauss, P., & Blöschl, G. (2019a). A Pedotransfer function for field-scale saturated hydraulic conductivity of a small watershed. *Vadose Zone Journal*, *18*(1), 1–15.

Picciafuoco, T., Morbidelli, R., Flammini, A., Saltalippi, C., Corradini, C., Strauss, P., & Blöschl, G. (2019b). On the estimation of spatially representative plot scale saturated hydraulic conductivity in an agricultural setting. *Journal of Hydrology*, *570*(1), 106–117. https://doi.org/10.1016/j.jhydrol.2018.12.044

Prosser, I. P., & Rustomji, P. (2004). Sediment transport capacity relations for overland flow. *Progress in Physical Geography*, *24*(2), 79–93.

Puckett, W. E., Dane, J. H., & Hajek, B. F. (1985). Physical and mineralogical data to determine soil hydraulic properties. *Soil Science Society of America Journal*, *49*(4), 831–836.

Quinton, J. N. (1994). The validation of physically-based erosion models — with particular reference to EUROSEM.

Quinton, J. N., Krueger, T., Freer, J., Brazier, R. E., & Bilotta, G. S. (2010). A Case Study of Uncertainty. In *Applying GLUE to EUROSEM. Handbook of Erosion Modelling* (pp. 80–97). Portico. https://doi.org/10.1002/9781444328455.ch5

Rauws, G., & Govers, G. (1988). Hydraulic and soil mechanical aspects of rill generation on agricultural soils. *Journal of Soil Science*, *39*(1), 111–124.

Reaney, S. M., Bracken, L. J., & Kirkby, M. J. (2014). The importance of surface controls on overland flow connectivity in semi-arid environments: Results from a numerical experimental approach. *Hydrological Processes*, *28*(4), 2116–2128.

Renard, K. G., Foster, G. R., Weesies, G. A., Mccool, D. K., & Yoder, D. C. (1997). Agricultural handbook No. 703 predicting soil erosion by water: A guide to conservation planning with the revised universal soil loss equation (RUSLE). http://www.ars.usda.gov/SP2UserFiles/Place/64080530/RUSLE/AH_703.pdf.

Saxton, K. E., & Rawls, W. J. (2006). Soil water characteristic estimates by texture and organic matter for Hydrologic solutions. *Soil Science Society of America Journal*, *70*(5), 1569–1578.

Saxton, K. E., Rawls, W. J., Romberger, J. S., & Papendick, R. I. (1986). Estimating generalized soil-water characteristics from texture. *Soil Science Society of America Journal*, *50*(4), 1031–1036.

Saxton, K. E., Willey, P. H., & Rawls, W. J. (2006). Field and pond HYDROLOGIC analyses with the SPAW model. In *ASAE annual meeting, ASABE paper No. 062108*. ASABE. https://elibrary.asabe.org/abstract.asp?aid=20709&t=5

Seibert, S. P., & Auerswald, K. (2020). *Hochwasserminderung Im Ländlichen Raum–Ein Handbuch Zur Quantitativen Planung*. Springer Spektrum Berlin.

Smith, H. G., Peñuela, A., Sangster, H., Sellami, H., Boyle, J., Chiverrell, R., Schillereff, D., & Riley, M. (2018). Simulating a century of soil erosion for agricultural catchment management. *Earth Surface Processes and Landforms*, *43*(10), 2089–2105.

Smith, R. E., & Parlange, J. Y. (1978). A parameter-efficient Hydrologic infiltration model. *Water Resources Research*, *14*(3), 533–538.

Sobol', I. M. (2001). Global sensitivity indices for nonlinear mathematical models and their Monte Carlo estimates I.M. *Mathematics and Computers in Simulation*, *55*, 271–280.

Stašek, J., Krása, J., Mistr, M., Dostál, T., Devátý, J., Středa, T., & Mikulka, J. (2023). Using a rainfall simulator to define the effect of soil conservation techniques on soil loss and water retention. *Land*, *12*(2), 431. https://doi.org/10.3390/land12020431

Sterk, G. (2021). A hillslope version of the revised Morgan, Morgan and Finney water erosion model. *International Soil and Water Conservation Research*, *9*(3), 319–332. https://doi.org/10.1016/j.iswcr.2021.01.004

Strauss, P., Auerswald, K., Klaghofer, E., & Blum, W. E. H. (1995). Erosivität von Niederschlägen: Ein Vergleich Österreich–Bayern. *Zeitschrift für Kulturtechnik Und Landentwicklung*, *36*, 304–308.

Strauss, P., Pitty, J., Pfeffer, M., & Mentler, A. (2000). Rainfall simulation for outdoor experiments. In P. Jamet & J. Cornejo (Eds.), *Current research methods to assess the environmental fate of pesticides* (pp. 329–333). INRA Editions.

Strohmeier, S., Laaha, G., Holzmann, H., & Klik, A. (2016). Magnitude and occurrence probability of soil loss: A risk analytical approach for the plot scale for two sites in Lower Austria. *Land Degradation and Development*, *27*(1), 43–51.

Szabó, B., Weynants, M., & Weber, T. K. D. (2021). Updated European hydraulic Pedotransfer functions with communicated uncertainties in the predicted variables (Euptfv2). *Geoscientific Model Development*, *14*(1), 151–175.

Tan, Z., Ruby Leung, L., Li, H. Y., & Tesfa, T. (2018). Modeling sediment yield in land surface and earth system models: Model comparison, development, and evaluation. *Journal of Advances in Modeling Earth Systems*, *10*(9), 2192–2213.

Torri, D., & Poesen, J. (2014). A review of topographic threshold conditions for gully head development in different environments. *Earth-Science Reviews*, *130*, 73–85. https://doi.org/10.1016/j.earscirev.2013.12.006

van Dijk, A. I. J. M., Bruijnzeel, L. A., & Rosewell, C. J. (2002). Rainfall intensity-kinetic energy relationships: A critical literature appraisal. *Journal of Hydrology*, *261*(1–4), 1–23.

Vente, D., Joris, J. P., Verstraeten, G., Govers, G., Vanmaercke, M., van Rompaey, A., Arabkhedri, M., & Boix-Fayos, C. (2013). Predicting soil erosion and sediment yield at regional scales: Where do we stand? *Earth-Science Reviews*, *127*, 16–29. https://doi.org/10.1016/j.earscirev.2013.08.014

Vereecken, H., Maes, J., & Feyen, J. (1990). Estimating unsaturated hydraulic conductivity from easily measured soil properties. *Soil Science*, *149*, 1–12.

Vieira, D. A. N., Dabney, S. M., & Yoder, D. C. (2014). Distributed soil loss estimation system including ephemeral gully development and tillage erosion. *IAHS-AISH Proceedings and Reports*, *367*(12), 80–86.

Vieira, D. C. S., Prats, S. A., Nunes, J. P., Shakesby, R. A., Coelho, C. O. A., & Keizer, J. J. (2014). Modelling runoff and erosion, and their mitigation, in burned Portuguese Forest using the revised Morgan-Morgan-Finney model. *Forest Ecology and Management*, *314*, 150–165. https://doi.org/10.1016/j.foreco.2013.12.006

Vigiak, O., Okoba, B. O., Sterk, G., & Groenenberg, S. (2005). Modelling catchment-scale erosion patterns in the east African highlands. *Earth Surface Processes and Landforms*, *30*(2), 183–196.

Wang, S., Peter Strauss, A., Yao, X. W., & Yuan, Y. (2018). Assessing hydrological connectivity development by using a photogrammetric technique with relative surface connection function (RSCf) in a plot-scale experiment. *Journal of Soil and Water Conservation*, *73*(5), 518–532.

Wang, S., Szeles, B., Krammer, C., Schmaltz, E., Song, K., Li, Y., Zhang, Z., Blöschl, G., & Strauss, P. (2022). Agricultural intensification vs. climate change: What drives long-term changes in sediment load? *Hydrology and Earth System Sciences*, *26*, 3021–3036.

Wang, S., Flanagan, D. C., & Engel, B. A. (2019). Estimating sediment transport capacity for overland flow. *Journal of Hydrology*, *578*(7), 123985. https://doi.org/10.1016/j.jhydrol.2019.123985

Weynants, M., Vereecken, H., & Javaux, M. (2009). Revisiting Vereecken pedotransfer functions: Introducing a closed-form hydraulic model. *Vadose Zone Journal*, *8*(1), 86–95.

Wischmeier, W. H., & Smith, D. D. (1978). *Agricultural handbook No. 537 predicting rainfall erosion losses–a guide to conservation planning*. Department of Agriculture, Science and Education Administration.

Woolhiser, D. A., Smith, R. E., & Goodrich, D. C. (1990). KINEROS: A kinematic runoff and erosion model: Documentation and user manual. In *ARS (series) (United States, Agricultural Research Service)* (p. 77). US Department of Agriculture, Agricultural Research Service.

Wösten, J. H. M., Lilly, A., Nemes, A., & le Bas, C. (1999). Development and use of a database of hydraulic properties of European soils. *Geoderma*, *90*(3), 169–185.

Wösten, J. H. M., Pachepsky, Y. A., & Rawls, W. J. (2001). Pedotransfer functions: Bridging the gap between available basic soil data and missing soil hydraulic characteristics. *Journal of Hydrology*, *251*(3–4), 123–150.

Zambon, N., Johannsen, L. L., Strauss, P., Dostal, T., Zumr, D., Cochrane, T. A., & Klik, A. (2021). Splash erosion affected by initial soil moisture and surface conditions under simulated rainfall. *Catena*, *196*(7), 104827. https://doi.org/10.1016/j.catena.2020.104827

Zhang, X. C., Nearing, M. A., Risse, L. M., & McGregor, K. C. (1996). Evaluation of WEPP runoff and soil loss predictions using natural runoff plot data. *Transactions of the American Society of Agricultural Engineers*, *39*(3), 855–863.

Zimbone, S. M., Vickers, A., Morgan, R. P. C., & Vella, P. (1996). Field investigations of different techniques for measuring surface soil shear strength. *Soil Technology*, *9*(1–2), 101–111.

SUPPORTING INFORMATION

Additional supporting information can be found online in the Supporting Information section at the end of this article.

How to cite this article: Brunner, T., Weninger, T., Schmaltz, E., Krasa, J., Stasek, J., Zavattaro, L., Sisak, I., Dostal, T., Klik, A., & Strauss, P. (2023). Testing CASE: A new event-based Morgan-Morgan-Finney-type erosion model for different rainfall experimental scenarios. *Hydrological Processes*, *37*(9), e14966. https://doi.org/10.1002/hyp.14966